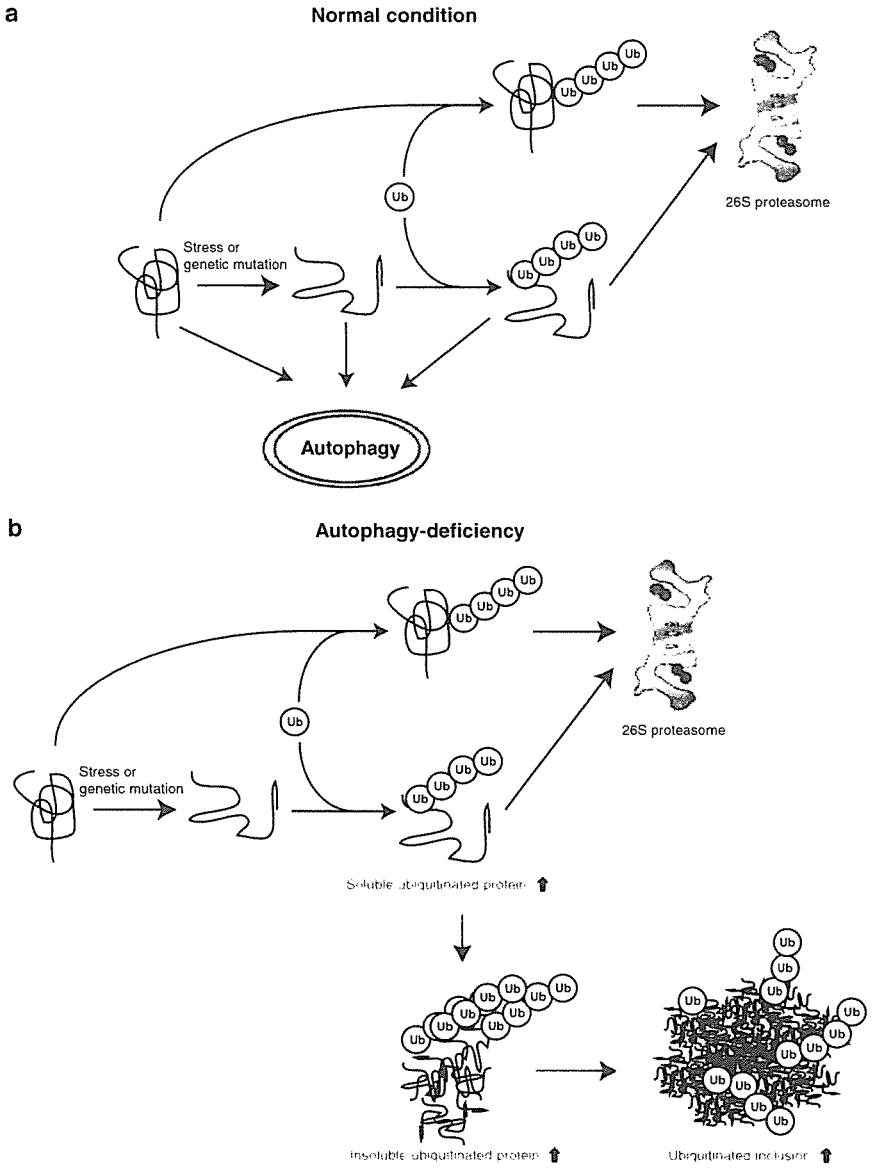

Figure 4 A schematic diagram of protein destruction pathways mediated by the proteasome and autophagy. The majority of cellular proteins, if not all, are polyubiquitylated before hydrolysis by the proteasome (an ATP-dependent proteolytic complex). Similarly, unfolded/misfolded proteins generated by environmental stresses or genetic mutations are discarded after polyubiquitylation by the same proteolytic system (**a**). Aging-related decline in autophagic activity causes accumulation of highly ubiquitylated proteins, which are recovered as both soluble and insoluble forms (**b**). As autophagy could feed both ubiquitylated and unubiquitylated protein(s), it is not clear at present whether polyubiquitylated aggregates/inclusions in autophagy-deficient neurons are formed consequent to impairment of degradation of unubiquitylated proteins or aggressively polyubiquitylated proteins. In addition, further work is needed to determine whether the two proteolytic systems (autophagy and proteasomes) work independently or cooperatively, and whether autophagy and the proteasome feed a similar set of normal and/or misfolded/unfolded proteins in general. Red text: protein dynamics associated with autophagy deficiency, Ub: ubiquitin

p62 plays a critical role in the formation of ubiquitin-positive aggregates by impaired autophagy (unpublished data). These results imply that ubiquitylated unfavorable proteins might be selectively sequestered into autophagosomes in part via p62 (which may retain its shuttling ability of ubiquitylated proteins). In either case (non-selective or selective degradation of ubiquitylated proteins by autophagy), our results indicate that autophagy operates not only as a supplier of amino acids under nutrient-poor conditions but also as a house cleaner of damaged proteins under nutrient-rich conditions.

Concluding Remarks

Considering the role of autophagy in neurodegenerative diseases, it is possible to align time-dependent enhancement and inactivation of autophagy. First, misfolded and/or

unfolded protein aggregates formed in neurons cause sequestration of mTor along with the aggregates, leading to significant inactivation of mTor, which stimulates autophagy (autophagosome formation). Second, if the size of aggregates is small enough and the degree of aggregation is moderate, the aggregates are engulfed into autophagosomal lumen and subsequently degraded via autophagy. Unless the amounts of aggregates surpass the clearance capacity of autophagosomes, maximal activation of autophagy by pharmaceutical agents such as rapamycin could be effective in preventing the progression of the disease. It is noteworthy that the expression of aggregation-prone protein(s) observed frequently in familial neurodegenerative disorders is not required for the formation of inclusions associated with impaired autophagy, suggesting the involvement of autophagy even in sporadic neurodegenerative diseases. On the other hand, autophagic activity of rat liver decreases with aging and this decrease conversely correlates with an increase in the accumulation of oxidized proteins.[36] Thus, age-dependent onset of neurodegenerative diseases most likely correlates with the age-dependent decline of autophagic activity. It is generally accepted that deficits of the proteasome-ubiquitin system are linked to various neurodegenerative disorders. Intriguingly, however, no obvious inhibition of the ubiquitin-proteasome system occurs in the mouse brain lacking autophagy, providing compelling evidence that constitutive autophagy plays a prominent role in neuronal survival, independent of proteasome function (Figure 4). In this context, we stress that proteasome inhibition induces augmented autophagy in order to eliminate unnecessary accumulated proteins, probably compensating the loss of proteasome functions.[22] Thus, the two major proteolytic pathways naturally differ in the cooperative responses in cells. We emphasize the importance of autophagy as a process with adaptive and flexible responses. Finally, a better understanding of basal or constitutive autophagy, which maintains basal activity of macroautophagy in neurons, may help in the design of new strategies to prevent neurodegenerative diseases.

1. Goldberg AL. Protein degradation and protection against misfolded or damaged proteins. *Nature* 2003; **426**: 895–899.
2. Levine B, Klionsky DJ. Development by self-digestion: molecular mechanisms and biological functions of autophagy. *Dev Cell* 2004; **6**: 463–477.
3. Cuervo AM. Autophagy: in sickness and in health. *Trends Cell Biol* 2004; **14**: 70–77.
4. Mizushima N, Ohsumi Y, Yoshimori T. Autophagosome formation in mammalian cells. *Cell Struct Funct* 2002; **27**: 421–429.
5. Takeshige K, Baba M, Tsuboi S, Noda T, Ohsumi Y. Autophagy in yeast demonstrated with proteinase-deficient mutants and conditions for its induction. *J Cell Biol* 1992; **119**: 301–311.
6. Mizushima N, Yamamoto A, Matsui M, Yoshimori T, Ohsumi Y. *In vivo* analysis of autophagy in response to nutrient starvation using transgenic mice expressing a fluorescent autophagosome marker. *Mol Biol Cell* 2004; **15**: 1101–1111.
7. Kabeya Y, Mizushima N, Ueno T, Yamamoto A, Kirisako T, Noda T *et al.* LC3, a mammalian homologue of yeast Apg8p, is localized in autophagosome membranes after processing. *EMBO J* 2000; **19**: 5720–5728.
8. Kabeya Y, Mizushima N, Yamamoto A, Oshitani-Okamoto S, Ohsumi Y, Yoshimori T. LC3, GABARAP and GATE16 localize to autophagosomal membrane depending on form-II formation. *J Cell Sci* 2004; **117**: 2805–2812.
9. Tanida I, Sou YS, Ezaki J, Minematsu-Ikeguchi N, Ueno T, Kominami E. HsAtg4B/HsApg4B/autophagin-1 cleaves the carboxyl termini of three human Atg8 homologues and delipidates microtubule-associated protein light chain 3- and GABAA receptor-associated protein-phospholipid conjugates. *J Biol Chem* 2004; **279**: 36268–36276.
10. Ichimura Y, Kirisako T, Takao T, Satomi Y, Shimonishi Y, Ishihara N *et al.* A ubiquitin-like system mediates protein lipidation. *Nature* 2000; **408**: 488–492.
11. Tanida I, Tanida-Miyake E, Ueno T, Kominami E. The human homolog of Saccharomyces cerevisiae Apg7p is a Protein-activating enzyme for multiple substrates including human Apg12p, GATE-16, GABARAP, and MAP-LC3. *J Biol Chem* 2001; **276**: 1701–1706.
12. Tanida I, Tanida-Miyake E, Komatsu M, Ueno T, Kominami E. Human Apg3p/Aut1p homologue is an authentic E2 enzyme for multiple substrates, GATE-16, GABARAP, and MAP-LC3, and facilitates the conjugation of hApg12p to hApg5p. *J Biol Chem* 2002; **277**: 13739–13744.
13. Mortimore GE, Hutson NJ, Surmacz CA. Quantitative correlation between proteolysis and macro- and microautophagy in mouse hepatocytes during starvation and refeeding. *Proc Natl Acad Sci USA* 1993; **80**: 2179–2183.
14. Komatsu M, Waguri S, Ueno T, Iwata J, Murata S, Tanida I *et al.* Impairment of starvation-induced and constitutive autophagy in Atg7-deficient mice. *J Cell Biol* 2005; **169**: 425–434.
15. Tsukada M, Ohsumi Y. Isolation and characterization of autophagy-defective mutants of Saccharomyces cerevisiae. *FEBS Lett* 1993; **333**: 169–174.
16. Kuma A, Hatano M, Matsui M, Yamamoto A, Nakaya H, Yoshimori T *et al.* The role of autophagy during the early neonatal starvation period. *Nature* 2004; **432**: 1032–1036.
17. Lum JJ, Bauer DE, Kong M, Harris MH, Li C, Lindsten T *et al.* Growth factor regulation of autophagy and cell survival in the absence of apoptosis. *Cell* 2005; **120**: 237–248.
18. Hollenbeck PJ. Products of endocytosis and autophagy are retrieved from axons by regulated retrograde organelle transport. *J Cell Biol* 1993; **121**: 305–315.
19. Puls I, Jonnakuty C, LaMonte BH, Holzbaur EL, Tokito M, Mann E *et al.* Mutant dynactin in motor neuron disease. *Nat Genet* 2003; **33**: 455–456.
20. Hafezparast M, Klocke R, Ruhrberg C, Marquardt A, Ahmad-Annuar A, Bowen S *et al.* Mutations in dynein link motor neuron degeneration to defects in retrograde transport. *Science* 2003; **300**: 808–812.
21. Ravikumar B, Acevedo-Arozena A, Imarisio S, Berger Z, Vacher C, O'Kane CJ *et al.* Dynein mutations impair autophagic clearance of aggregate-prone proteins. *Nat Genet* 2005; **37**: 771–776.
22. Iwata A, Riley BE, Johnston JA, Kopito RR. HDAC6 and microtubules are required for autophagic degradation of aggregated huntingtin. *J Biol Chem* 2005; **280**: 40282–40292.
23. Okamoto K, Hirai S, Iizuka T, Yanagisawa T, Watanabe M. Reexamination of granulovacuolar degeneration. *Acta Neuropathol (Berlin)* 1991; **82**: 340–345.
24. Cataldo AM, Hamilton DJ, Barnett JL, Paskevich PA, Nixon RA. Properties of the endosomal-lysosomal system in the human central nervous system: disturbances mark most neurons in populations at risk to degenerate in Alzheimer's disease. *J Neurosci* 1996; **16**: 186–199.
25. Anglade P, Vyas S, Javoy-Agid F, Herrero MT, Michel PP, Marquez J *et al.* Apoptosis and autophagy in nigral neurons of patients with Parkinson's disease. *Histol Histopathol* 1997; **12**: 25–31.
26. Kegel KB, Kim M, Sapp E, McIntyre C, Castano JG, Aronin N *et al.* Huntingtin expression stimulates endosomal-lysosomal activity, endosome tubulation, and autophagy. *J Neurosci* 2000; **20**: 7268–7278.
27. Petersen A, Larsen KE, Behr GG, Romero N, Przedborski S, Brundin P *et al.* Expanded CAG repeats in exon 1 of the Huntington's disease gene stimulate dopamine-mediated striatal neuron autophagy and degeneration. *Hum Mol Genet* 2001; **10**: 1243–1254.
28. Tanida I, Minematsu-Ikeguchi N, Ueno T, Kominami E. Lysosomal turnover, but not a cellular level, of endogenous LC3 is a marker for autophagy. *Autophagy* 2005; **1**: 84–91.
29. Nishino I, Fu J, Tanji K, Yamada T, Shimojo S, Koori T *et al.* Primary LAMP-2 deficiency causes X-linked vacuolar cardiomyopathy and myopathy (Danon disease). *Nature* 2000; **406**: 906–910.
30. Tanaka Y, Guhde G, Suter A, Eskelinen EL, Hartmann D, Lullmann-Rauch R *et al.* Accumulation of autophagic vacuoles and cardiomyopathy in LAMP-2-deficient mice. *Nature* 2000; **406**: 902–906.
31. Ikeda H, Yamaguchi M, Sugai S, Aze Y, Narumiya S, Kakizuka A. Expanded polyglutamine in the Machado–Joseph disease protein induces cell death *in vitro* and *in vivo*. *Nat Genet* 1996; **13**: 196–202.
32. Sanchez I, Mahlke C, Yuan J. Pivotal role of oligomerization in expanded polyglutamine neurodegenerative disorders. *Nature* 2003; **421**: 373–379.
33. Arrasate M, Mitra S, Schweitzer ES, Segal MR, Finkbeiner S. Inclusion body formation reduces levels of mutant huntingtin and the risk of neuronal death. *Nature* 2004; **431**: 805–810.
34. Ravikumar B, Duden R, Rubinsztein DC. Aggregate-prone proteins with polyglutamine and polyalanine expansions are degraded by autophagy. *Hum Mol Genet* 2002; **11**: 1107–1117.
35. Inoki K, Corradetti MN, Guan KL. Dysregulation of the TSC-mTOR pathway in human disease. *Nat Genet* 2005; **37**: 19–24.
36. Bergamini E. Autophagy: a cell repair mechanism that retards ageing and age-associated diseases and can be intensified pharmacologically. *Mol Aspects Med* 2006; **27**: 403–410.
37. Ravikumar B, Vacher C, Berger Z, Davies JE, Luo S, Oroz LG *et al.* Inhibition of mTOR induces autophagy and reduces toxicity of polyglutamine expansions in fly and mouse models of Huntington disease. *Nat Genet* 2004; **36**: 585–595.
38. Yamamoto A, Cremona ML, Rothman JE. Autophagy-mediated clearance of huntingtin aggregates triggered by the insulin-signaling pathway. *J Cell Biol* 2006; **172**: 719–731.
39. Wilson CA, Murphy DD, Giasson BI, Zhang B, Trojanowski JQ, Lee VM. Degradative organelles containing mislocalized alpha-and beta-synuclein proliferate in presenilin-1 null neurons. *J Cell Biol* 2004; **165**: 335–346.

40. Esselens C, Oorschot V, Baert V, Raemaekers T, Spittaels K, Serneels L *et al.* Presenilin 1 mediates the turnover of telencephalin in hippocampal neurons via an autophagic degradative pathway. *J Cell Biol* 2004; **166**: 1041–1054.
41. Yu WH, Cuervo AM, Kumar A, Peterhoff CM, Schmidt SD, Lee JH *et al.* Macroautophagy – a novel Beta-amyloid peptide-generating pathway activated in Alzheimer's disease. *J Cell Biol* 2005; **171**: 87–98.
42. Jenner P, Olanow CW. Understanding cell death in Parkinson's disease. *Ann Neurol* 1998; **44**: S72–S84.
43. Kruger R, Kuhn W, Muller T, Woitalla D, Graeber M, Kosel S *et al.* Ala30Pro mutation in the gene encoding alpha-synuclein in Parkinson's disease. *Nat Genet* 1998; **18**: 106–108.
44. Polymeropoulos MH, Lavedan C, Leroy E, Ide SE, Dehejia A, Dutra A *et al.* Mutation in the alpha-synuclein gene identified in families with Parkinson's disease. *Science* 1997; **276**: 2045–2047.
45. Chung KK, Dawson VL, Dawson TM. The role of the ubiquitin-proteasomal pathway in Parkinson's disease and other neurodegenerative disorders. *Trends Neurosci* 2001; **24**: S7–S14.
46. Mouradian MM. Recent advances in the genetics and pathogenesis of Parkinson disease. *Neurology* 2002; **58**: 179–185.
47. Stefanis L, Larsen KE, Rideout HJ, Sulzer D, Greene LA. Expression of A53T mutant but not wild-type alpha-synuclein in PC12 cells induces alterations of the ubiquitin-dependent degradation system, loss of dopamine release, and autophagic cell death. *J Neurosci* 2001; **21**: 9549–9560.
48. Webb JL, Ravikumar B, Atkins J, Skepper JN, Rubinsztein DC. Alpha-Synuclein is degraded by both autophagy and the proteasome. *J Biol Chem* 2003; **278**: 25009–25013.
49. Cuervo AM, Stefanis L, Fredenburg R, Lansbury PT, Sulzer D. Impaired degradation of mutant alpha-synuclein by chaperone-mediated autophagy. *Science* 2004; **305**: 1292–1295.
50. Komatsu M, Waguri S, Chiba T, Murata S, Iwata J, Tanida I *et al.* Loss of autophagy in the central nervous system causes neurodegeneration in mice. *Nature* 2006; **441**: 880–884.
51. Hara T, Nakamura K, Matsui M, Yamamoto A, Nakahara Y, Suzuki-Migishima R *et al.* Suppression of basal autophagy in neural cells causes neurodegenerative disease in mice. *Nature* 2006; **441**: 885–889.
52. Bjorkoy G, Lamark T, Brech A, Outzen H, Perander M, Overvatn A *et al.* p62/SQSTM1 forms protein aggregates degraded by autophagy and has a protective effect on huntingtin-induced cell death. *J Cell Biol* 2005; **171**: 603–614.

BRAIN RESEARCH 1073–1074 (2006) 93–102

available at www.sciencedirect.com

SCIENCE DIRECT®

www.elsevier.com/locate/brainres

BRAIN RESEARCH

Short Communication

Localization of Id2 mRNA in the adult mouse brain

Kazuhito Kitajima[a,b,c], *Ryosuke Takahashi*[c], *Yoshifumi Yokota*[a,]

[a]*Department of Molecular Genetics, School of Medicine, University of Fukui, 23-3 Shimoaizuki, Matsuoka, Fukui 910-1193, Japan*
[b]*Department of Neurology, Fukui Red Cross Hospital, 2-4-1 Tsukimi, Fukui 918-8501, Japan*
[c]*Department of Neurology, Graduate School of Medicine, Kyoto University, 54 Shogoin Kawahara-cho, Sakyo 606-8507, Kyoto, Japan*

ARTICLE INFO

Article history:
Accepted 12 December 2005
Available online 27 January 2006

Keywords:
Helix–loop–helix protein
Id2
Gene expression
Adult brain
Mouse

Abbreviations:
bHLH, basic helix–loop–helix
HLH, helix–loop–helix
DEPC, diethylpyrocarbonate

ABSTRACT

Id proteins are negative regulators of basic helix–loop–helix transcription factors and are involved in cellular differentiation and proliferation. Four members of the Id gene family exhibit closely related but distinct expression patterns in various mammalian organs of not only embryos but also adults. Among them, Id2 is known to be expressed in Purkinje cells and neurons in the cortical layers of the adult mouse brain, suggesting that Id2 is involved in some neural functions in the adult. To get insight into the role of Id2 in the nervous system, we investigated the localization of Id2 mRNA-expressing cells in the adult mouse brain in detail by in situ hybridization with the radiolabeled antisense probe and compared it with the localization of other Id gene family members. The results indicated that Id2 mRNA is detected in more varied brain regions than previously reported. These regions include the amygdaloid complex, caudate putamen, globus pallidus, substantia nigra pars reticulata, suprachiasmatic nucleus, and the anterior part of the subventricular zone. These results suggest the possibility that Id2 plays a role in the neural activity and cognitive functions. On the other hand, Id1 was barely detectable. Although moderate or low expression of Id3 was observed diffusely, high expression was observed in some specific regions including the molecular layer of the dentate gyrus and the external capsule. Id4 mRNA was detected in the regions such as the caudate putamen and the lateral amygdaloid nucleus. Thus, the expression pattern of Id2 is distinct from those of other Id gene family members.

Transcription factors play essential roles in various biological processes including cellular differentiation and proliferation by regulating gene expression. They are categorized according to their structural similarities. The basic helix–loop–helix (bHLH) protein family is a typical example. The members of this family share structural characteristics of the basic region and the helix–loop–helix (HLH) domain, which are required for DNA binding and dimerization, respectively (Massari and Murre, 2000). In general, tissue-specific bHLH factors form heterodimers with ubiquitously expressed bHLH factors, so-called E proteins consisting of E2A gene products (E12 and E47), HEB and E2-2, and regulate the expression of their respective target genes via the consensus-binding site, the E box (Massari and Murre, 2000). Tissue-specific bHLH factors that exhibit a high degree of sequence conservation constitute subfamilies and are involved in similar biological processes (Kageyama and Nakanishi, 1997; Massari and Murre, 2000). For example, neurogenic bHLH factors, such as NeuroD and Mash1, play

Corresponding author. Fax: +81 776 61 8164.
E-mail address: yyokota@fmsrsa.fukui-med.ac.jp (Y. Yokota).

0006-8993/$ – see front matter © 2005 Elsevier B.V. All rights reserved.
doi:10.1016/j.brainres.2005.12.048

important roles in cell fate determination, specification and proliferation control during neurogenesis in a wide variety of species by constituting gene regulatory cascades and carrying out their specific functions (Kageyama and Nakanishi, 1997; Massari and Murre, 2000).

Id proteins, inhibitors of DNA binding/differentiation, are negative regulators of bHLH transcription factors, and four members of this protein family, Id1–Id4, have been identified in mammals (Massari and Murre, 2000; Ruzinova and Benezra, 2003). They possess HLH domains and form heterodimers with bHLH factors, but the resultant heterodimers are unable to bind DNA due to the lack of a DNA-binding domain in Id proteins (Massari and Murre, 2000; Ruzinova and Benezra, 2003). Thus, Id proteins inhibit the functions of bHLH factors in a dominant negative manner and suppress bHLH factor-dependent cellular differentiation (Massari and Murre, 2000; Ruzinova and Benezra, 2003). On the other hand, Id proteins have the ability to stimulate cell cycle progression. Although the mechanism remains unclear, Id proteins have been reported to have abilities to inhibit the enhanced expression of cyclin-dependent inhibitors such as p21 by bHLH factors and to antagonize the activity of Rb family proteins (Ruzinova and Benezra, 2003; Yokota and Mori, 2002). Based on these functional characteristics, Id proteins are thought to be involved in the regulation of cell differentiation and in the expansion of immature cell populations (Ruzinova and Benezra, 2003; Yokota and Mori, 2002). In fact, each member of the Id gene family is expressed in a wide range of embryonic tissues including the central nervous system, and different members show similar but distinct expression patterns (Andres-Barquin et al., 2000; Jen et al., 1996, 1997; Neuman et al., 1991; Rubenstein et al., 1999; Tzeng and de Vellis, 1998). Id genes are also expressed in the adult central nervous system (Andres-Barquin et al., 2000; Elliott et al., 2001; Neuman et al., 1991; Riechmann et al., 1994; Rubenstein et al., 1999; Tzeng and de Vellis, 1998), although there is a tendency for the expression levels to decrease (Andres-Barquin et al., 2000; Neuman et al., 1991; Tzeng and de Vellis, 1998). For example, Id2 is expressed in neurons in all layers of the cerebral cortex except layer 4, Purkinje cells of the cerebellum, the olfactory bulb (the mitral cell, glomerular and internal granule cell layers), the hippocampus, and the suprachiasmatic nucleus (SCN) of the adult rodent brain (Andres-Barquin et al., 2000; Elliott et al., 2001; Neuman et al., 1991; Rubenstein et al., 1999; Tzeng and de Vellis, 1998; Ueda et al., 2002). These observations suggest that Id proteins are involved in cellular functions in terminally differentiated and non-dividing cells, in addition to playing roles in cell differentiation and proliferation control.

To get insight into the role of Id2 in neural functions, we investigated the distribution of Id2 mRNA in the adult mouse brain by in situ hybridization. Adult male mice of ICR or the mixed genetic background between NMRI and 129/Sv were used in this study. Similar results were obtained from the two strains. Mice were deeply anesthetized with diethyl ether and perfused transcardially with PBS followed by fixative containing 4% paraformaldehyde in PBS. After perfusion, the brain was taken out of the skull, immersed in the same fixative for 24 h at 4 °C, transferred to 0.1% diethylpyrocarbonate (DEPC)-treated 20% sucrose in PBS for 48 h at 4 °C, and then frozen with OCT compound at −80 °C. The brain was cut into 10- m-thick sections on a cryostat and mounted on glass slides. Sections were stored at −80 °C until use. All animal procedures were performed in accordance with the guidelines of the University of Fukui for animal experiments. In situ hybridization was performed as described (Ishii et al., 1990; Mori et al., 2000). Briefly, 10- m-thick coronal sections were treated with 5 g/ml proteinase K and acetylated before hybridization. An ^{35}S-labeled RNA probe spanning nt 61–759 of the mouse Id2 cDNA was generated by transcription with RNA polymerase using the pBS-Id2 plasmid as template (Mori et al., 2000). The sections were hybridized in the presence of 50% formamide at 60 °C overnight, washed at high stringency, dipped with NTB2 emulsion (Kodak), and autoradiographed. The sections were then counterstained with the Cresyl Fast Violet solution to allow morphological identification. Anatomical determinations were made according to a standard atlas (Paxinos and Franklin, 2001). In situ hybridization of brain sections with the ^{35}S-labeled sense probe gave no appreciable signal and confirmed the specificity of the ^{35}S-labeled antisense probe for the detection of the Id2 mRNA (data not shown).

In the main olfactory bulb, Id2 mRNA was expressed in the mitral, glomerular, and granule cell layers (Mi, Gl, GrO) (Fig. 1A and Table 1), as reported (Neuman et al., 1991). In the anterior olfactory nucleus, both medial (AOM) and posterior (AOP) parts were stained (Fig. 1B). In the septum, Id2 mRNA was moderately expressed in the lateral septal nucleus, intermediate and ventral part (LSI and LSV, respectively) (Fig. 1C), although the expression level was lower in the lateral septal nucleus, dorsal part (LSD), and medial septal nucleus (MS) (Fig. 1C). Some Id2-expressing cells were distributed in the corpus callosum (cc) (Figs. 1C, 3E), in accordance with the report about Id2 mRNA expression in S100$^+$GFAP$^+$ astrocytes and GFAP$^-$ and O4$^-$ cells in the rat corpus callosum (Tzeng and de Vellis, 1998).

In the cerebral cortex, Id2 mRNA was detected in all layers except layer 4, and scattered cells were positive for Id2 mRNA in layer 1 (Figs. 1B–G, 2A–C). Strong Id2 mRNA expression was observed in layer 5 of the neocortex as reported (Figs. 1C–F) and in layer 2 in the piriform cortex (Pir) (Figs. 1B–D). In the cingulate (Cg/RS) and retrosplenial cortices (RS), the level of Id2 mRNA expression was high in layers 2 and 3 (Figs. 1E and F).

Strong expression of Id2 mRNA was observed in the many regions of the amygdaloid complex: the basolateral amygdaloid nucleus anterior part (BLA), lateral amygdaloid nucleus dorsolateral part (LaDL), ventromedial part (LaVM), ventrolateral part (LaVL), medial amygdaloid nucleus posterodorsal part (MePD), posteroventral part (MePV), posteromedial cortical amygdaloid nucleus (PMCo), and intercalated nuclei of the amygdala (I) (Figs. 1D–G and 3A). In the other subnuclei, moderately expressing cells were distributed (Fig. 3A). In addition, moderate expression was observed in the dorsal and ventral parts of the anterior amygdaloid area (AAD, AAV), anterior cortical amygdaloid nucleus (ACo), and nucleus of the lateral olfactory tract (LOT) (Fig 1D). High expression was also seen in the dorsal endopiriform nucleus (DEn) (Figs. 1B and F, 3A). Moderate expression was also observed in the bed nucleus of stria terminalis (BST) (Fig. 1D) and the intraamygdaloid division of the bed nucleus of the stria terminalis

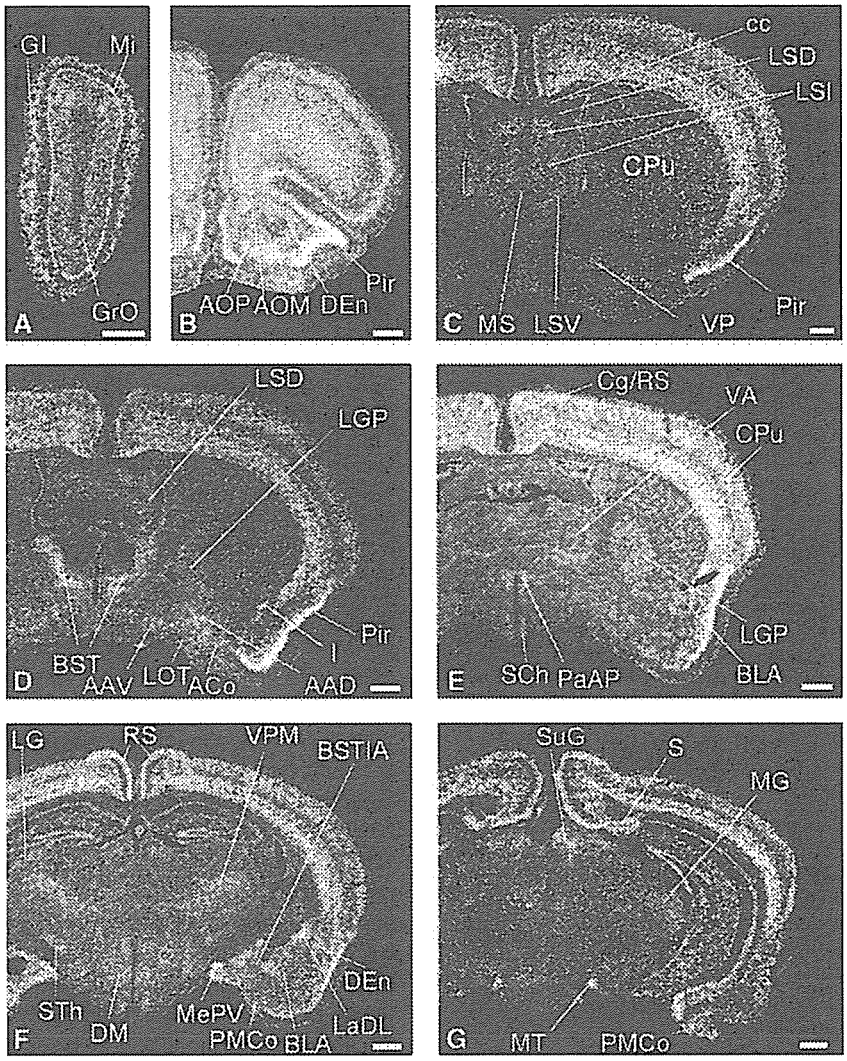

Fig. 1 – Expression of Id2 mRNA in the forebrain and thalamus. Dark field photomicrographs showing Id2 mRNA expression in coronal sections. Strong expression was observed in the piriform cortex (B) (C), bed nucleus of the stria terminalis, intercalated nuclei of the amygdala (D), cingulate/retrosplenial cortex (E), dorsal endopiriform nucleus, lateral amygdaloid nucleus dorsolateral part, medial amygdaloid nucleus posterodorsal part (F), subiculum, superficial gray layer of the superior colliculus, and medial terminal nucleus of the accessory optic tract (G). Scale bar, 500 m. Abbreviations are listed in Table 1.

(BSTIA) (Fig. 1F). Cells expressing Id2 mRNA moderately or strongly were dispersed throughout the hippocampus. It has been reported that Id2-expressing cells in the hippocampus are interneurons and/or glial cells (Elliott et al., 2001). Id2 positive cells were found in subgranular zone (SGZ) of the dentate, but most of the granule cells and pyramidal cells were not labeled (Fig. 3B). Id2 mRNA was clearly detectable in the subiculum (S) (Figs. 1G, 2A and B). Macroscopic observation of the sections demonstrated that the globus pallidus showed the strongest reactivity in the basal ganglia. In the microscopic study of the globus pallidus, most cells were moderately labeled for Id2 mRNA (LGP) (Fig. 1E). Although medium- to large-sized neurons and some glial cells were moderately labeled in the caudate putamen, the majority of striatal neurons were not positive for Id2 expression (Figs. 1C–E and 3C).

In the subventricular zone (SVZ) and ependymal region, some cells were labeled (Fig. 3E). In the anterior part of the subventricular zone (SVZa), which is a source of neuronal progenitor cells for the olfactory bulb (Luskin, 1993), strongly labeled cells were detected (Fig. 3F). In ventral pallidum (VP), moderately labeled cells were detected (Fig. 1C).

Id2 mRNA was expressed in some thalamic subnuclei: moderate expression was seen in the ventral anterior thalamic nucleus (VA) and ventral posteromedial thalamic nucleus (VPM) and weak expression in other regions (Figs. 1E and F). Moderate Id2 expression was detected in the lateral and medial geniculate nucleus (LG, MG) (Figs. 1F and G) and in the subthalamic nucleus (STh) (Fig. 1F). Id2 mRNA was also moderately expressed in the suprachiasmatic nuclei (SCh) (Figs. 1E and 3D), paraventricular hypothalamic nucleus anterior parvicellular part (PaAP) (Fig. 1E), and dorsomedial hypothalamic nucleus (DM) (Fig. 1F). In other nuclei located in this area, the expression level was weak or undetectable (Fig. 1E).

Table 1 – Abbreviations

3N	Oculomotor nucleus
4N	Trochlear nucleus
10N	Dorsal motor nucleus of vagus
12N	Hypoglossal nucleus
AAD	Anterior amygdaloid area, dorsal part
AAV	Anterior amygdaloid area, ventral part
aci	Anterior commissure, intrabulbar part
ACo	Anterior cortical amygdaloid nucleus
AOM	Anterior olfactory nucleus, medial part
AOP	Anterior olfactory nucleus, posterior part
BLA	Basolateral amygdaloid nucleus, anterior part
BST	Bed nucleus of the stria terminalis
BSTIA	Bed nucleus of the stria terminalis, intraamygdaloid division
cc	Corpus callosum
cg	Cingulum
Cg/RS	Cingulate/retrosplenial cortex
CPu	Caudate putamen
DC	Dorsal cochlear nucleus
DEn	Dorsal endopiriform nucleus
DM	Dorsomedial hypothalamic nucleus
DR	Dorsal raphe nucleus
DRD	Dorsal raphe nucleus, dorsal part
DRV	Dorsal raphe nucleus, ventral part
ec	External capsule
Gl	Glomerular layer of the olfactory bulb
GrO	Granular cell layer of the olfactory bulb
hbc	Habenular commissure
I	Intercalated nuclei of the amygdala
ic	Internal capsule
InG	Intermediate gray layer of the superior colliculus
Int	Interposed cerebellar nucleus,
IP	Interpeduncular nucleus
IPL	Interpeduncular nucleus, lateral subnucleus
IPR	Interpeduncular nucleus, rostral subnucleus
LaDL	Lateral amygdaloid nucleus, dorsolateral part
Lat	Lateral dentate cerebellar nucleus
LaVL	Lateral amygdaloid nucleus, ventrolateral part
LaVM	Lateral amygdaloid nucleus, ventromedial part
LG	Lateral geniculate nucleus
LGP	Lateral globus pallidus
ll	Lateral lemniscus
LOT	Nucleus of the lateral olfactory tract
LPGi	Lateral paragigantocellular nucleus
LSD	Lateral septal nucleus, dorsal part
LSI	Lateral septal nucleus, intermediate part
LSO	Lateral superior olive
LSV	Lateral septal nucleus, ventral part
LVe	Lateral vestibular nucleus
MePD	Medial amygdaloid nucleus, posterodorsal part
MePV	Medial amygdaloid nucleus, posteroventral part
MG	Medial geniculate nucleus
MHb	Medial habenular nucleus
Mi	Mitral cell layer of the olfactory bulb
MnR	Median raphe nucleus
Mo5	Motor trigeminal nucleus
Mol	Molecular layer of the dentate gyrus
MS	Medial septal nucleus
MT	Medial terminal nucleus of the accessory Optic tract
PaAP	Paraventricular hypothalamic nucleus, anterior parvicellular part
PAG	Periaqueductal gray
Pir	Piriform cortex
PMCo	Posteromedial cortical amygdaloid nucleus (C3)
Pn	Pontine nuclei
PnO	Pontine reticular nucleus, oral part
Po	Posterior thalamic nuclear group
PO	Periolivary region
Pr5	Principal sensory trigeminal nucleus
RMC	Red nucleus, magnocellular part
RPO	Rostral periolivary region
RS	Retrosplenial cortex
RVL	Rostroventrolateral reticular nucleus
S	Subiculum
SCh	Suprachiasmatic nucleus
sm	Stria medullaris of the thalamus
SNR	Substantia nigra, reticular part
Sp5	Spinal trigeminal nucleus
st	Stria terminalis
STh	Subthalamic nucleus
SuG	Superficial gray layer of the superior colliculus
TS	Triangular septal nucleus
Tz	Nucleus of the trapezoid body
VA	Ventral anterior thalamic nucleus
VC	Ventral cochlear nucleus
VP	Ventral pallidum
VPL	Ventral posterolateral thalamic nucleus
VPM	Ventral posteromedial thalamic nucleus

While most cells in the pars reticulata of the substantia nigra (SNR) were moderately labeled for Id2 mRNA, no signals were detected in the pars compacta, pars lateralis, or ventral tegmental area (Fig. 2A). Moderate expression was observed in the interpeduncular nucleus (IP) (Fig. 2A). Strongly labeled cells were seen in the medial terminal nucleus of the accessory optic tract (MT) (Fig. 1G). Moderate Id2 mRNA expression was detected in the red nucleus, magnocellular part (RMC) (Fig. 2A). Id2 mRNA was expressed moderately in the superficial gray layer of the superior colliculus (SuG) and weakly in the oculomotor nucleus (3N), the trochlear nucleus (4N) and the intermediate gray layer of the superior colliculus (InG) (Figs. 2A and B).

In the pons, Id2 mRNA was strongly expressed in the pontine nucleus (Pn), while weak expression was observed in the median raphe nucleus (MnR), dorsal raphe nucleus (DR), periaqueductal gray (PAG), and pontine reticular nucleus, oral part (PnO) (Fig. 2B). Id2 mRNA was expressed strongly in the nucleus of lateral lemniscus (ll), rostral periolivary region (RPO), and the ventral and dorsal cochlear nuclei (VC, DC) and moderately in the nucleus of the trapezoid body (Tz), lateral superior olive (LSO), and periolivary region (PO) (Figs. 2C, D, and E). Id2 mRNA was weakly expressed in the motor trigeminal nucleus (Mo5) and principal sensory trigeminal nucleus (Pr5) (Fig. 2D). In the medulla, moderately labeled cells were found in the dorsal motor nucleus of the vagus (10N) (Fig. 2F). Id2 mRNA was weakly expressed in the hypoglossal nucleus (12N), lateral paragigantocellular nucleus (LPGi), spinal trigeminal nucleus (Sp5), and rostroventrolateral reticular nucleus (RVL) (Fig. 2F) In the cerebellum, Id2 was strongly expressed in Purkinje cells, but not in the external granule, molecular, or internal granule cell layers at 8 weeks old of age (Fig. 2E). The cells in the cerebellar nuclei (Int, Lat) showed moderate expression of Id2 mRNA (Fig. 2E). The lateral vestibular nucleus (LVe) displayed moderate expression of Id2 (Fig. 2E).

Northern blot analysis has revealed that the expression level of Id2 in the adult mouse brain is similar to that in the embryonic brain (Andres-Barquin et al., 2000; Neuman et al.,

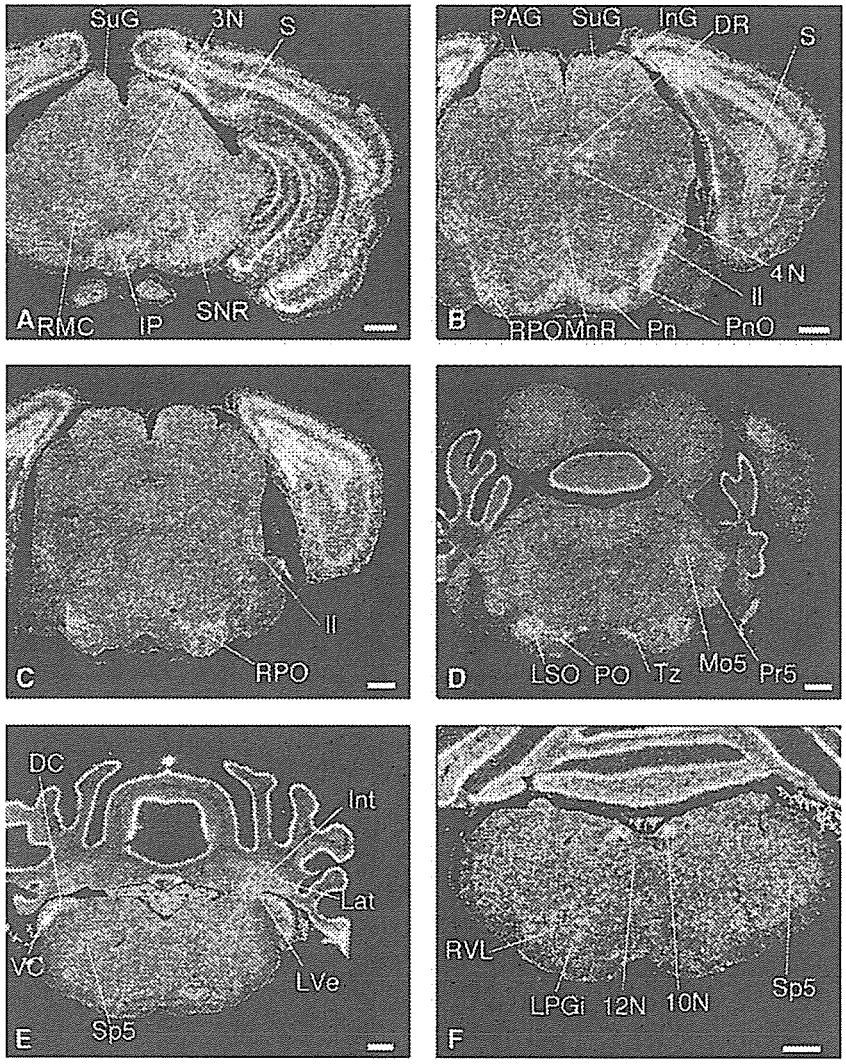

Fig. 2 – Expression of Id2 mRNA in the brainstem. Dark field photomicrographs showing Id2 mRNA expression in coronal sections. Strong expression was observed in the pontine nuclei, lateral lemniscus (B), dorsal and ventral cochlear nucleus (E), and dorsal motor nucleus of vagus (F). Scale bar, 500 m. Abbreviations are listed in Table 1.

1991). We examined the regional expression level of Id2 in the adult mouse brain. Total RNA was purified from the cerebral cortex, cerebellum, and caudate putamen of the adult mouse brain. Twenty micrograms of total RNA was separated by electrophoresis on a 1.0% agarose-formaldehyde gel, transferred onto filters, and cross-linked in a UV chamber. Hybridization with the probe derived from the full-length Id2 cDNA and washing were performed under high stringency conditions as described (Mori et al., 2000). X-ray films were exposed with an intensifying screen at –80 °C for 72 h. As shown in Fig. 3G, Id2 expression was high in the cerebral cortex and cerebellum and low in the caudate putamen.

The Id gene family consists of 4 members, Id1–Id4. To examine the difference of their expression patterns in the adult mouse brain, we performed in situ hybridization with the respective radiolabeled probes. The probes for Id1, Id3, and Id4 corresponded to the regions spanning nt 1–927, nt 560–969, and nt 2927–4701 of the respective cDNAs (Benezra et al., 1990; Christy et al., 1991; Riechmann et al., 1994). Since no apparent signal was detected for Id1 mRNA, we show the results for the expression of Id3 and Id4 mRNAs. Although Id3 mRNA was detected in many brain regions at a low or moderate level, some specific regions showed higher expression. In the main olfactory bulb, Id3 mRNA was expressed in the glomerular layer (Gl) (Fig. 4A). In the septum, Id3 mRNA was expressed in the medial septal nucleus (MS) and triangular septal nucleus (TS) (Figs. 4B and C). In the stria medullaris of the thalamus (sm), stria terminalis (st), habenular commissure (hbc), and medial habenular nucleus (MHb), Id3 mRNA was moderately expressed (Figs. 4C and D). Some Id3-expressing cells were also distributed in the corpus callosum (cc), external and internal capsule (ec, ic), and cingulum (cg) (Figs. 4B, D, and E). In the cerebral cortex, Id3 mRNA was detected in layers 5 and 6, and scattered cells were positive for Id3 mRNA in layer 1 (Figs. 4B–E). Some cells were moderately labeled in the caudate putamen (CPu) and lateral globus pallidus (LGP) (Figs. 4B and C). In the SVZ–ependymal region, some cells were labeled (Fig. 8B). In the hippocampus, Id3 was expressed in the molecular layer of the dentate gyrus (Mol) (Figs. 4D and E). Moderately labeled cells were scattered in the posterior thalamic nuclear

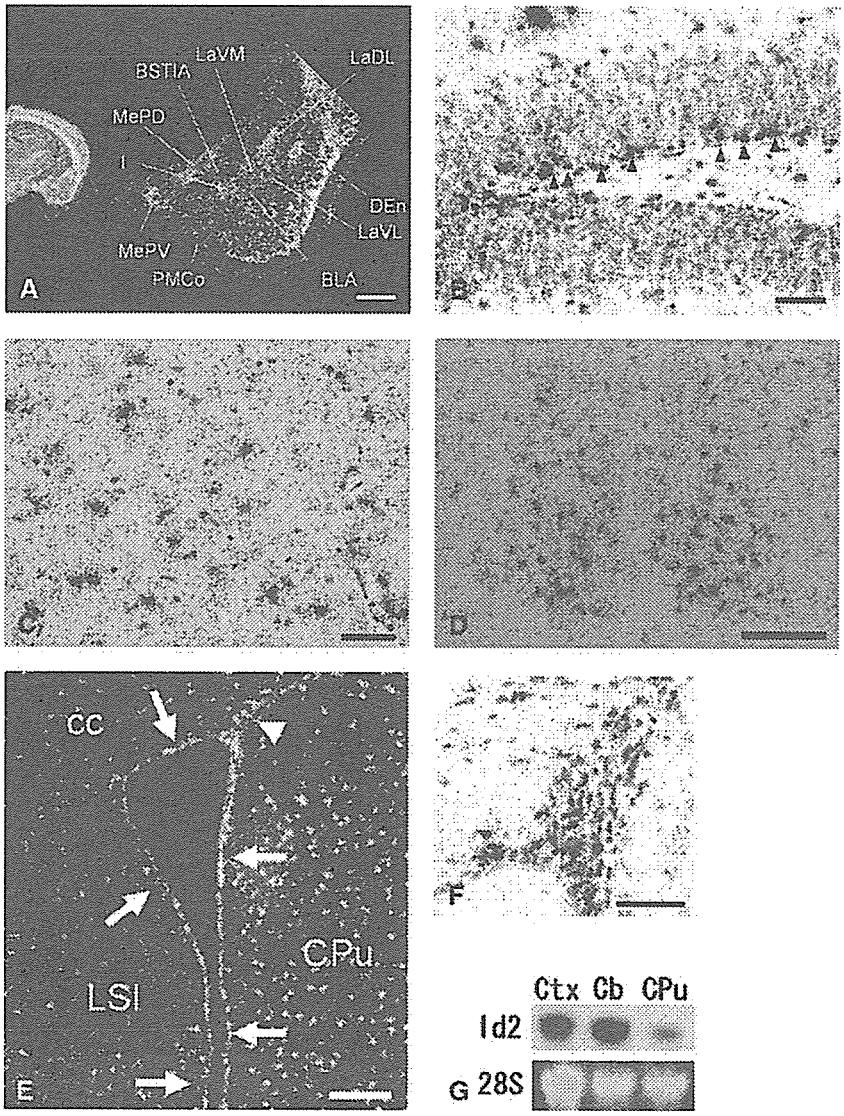

Fig. 3 – Expression of Id2 mRNA in the brain regions. (A) Dark field photomicrographs showing Id2 mRNA expression in the amygdala. Coronal sections. High magnification of the area indicated by a square is shown on the right. Id2 mRNA expression was observed widely in the subnuclei in the amygdala. Strong expression was observed in the dorsal endopiriform nucleus, lateral amygdaloid nucleus dorsolateral part and ventromedial part, medial amygdaloid nucleus posterodorsal part and posteroventral part, intercalated nuclei. Scale bar, 500 m. Abbreviations are listed in Table 1. (B) Bright field photomicrograph showing high magnification of the granule layer and subgranular zone of the hippocampus. Note that Id2 mRNA was detected in the subgranular zone of the dentate where neurogenesis is known to occur (arrowheads). Most of the granule cells and pyramidal cells were not labeled. Scale bar, 50 m. (C) Bright field photomicrograph showing Id2 mRNA expression in the caudate putamen. Strongly labeled cells were scattered sparsely in the caudate putamen. Scale bar, 100 m. (D) Bright field photomicrograph showing Id2 mRNA expression in the suprachiasmatic nucleus. Scale bar, 200 m. (E) Dark field photomicrograph showing the expression of Id2 mRNA in the subventricular zone–ependymal region (arrow) and anterior part of the subventricular zone (SVZa) (arrowhead). Scale bar, 200 m. Abbreviations are listed in Table 1. (F) Bright field photomicrograph showing higher magnification of SVZa. Scale bar, 100 m. (G) Northern blot analysis for Id2 expression. Total RNA was isolated from the cerebral cortex (Ctx), cerebellum (Cb), and caudate putamen (CPu) of the adult mouse brain and subjected to Northern blotting. Twenty-eight S ribosomal RNA is shown as a loading control.

group (Po), ventral posteromedial thalamic nucleus (VPM), and ventral posterolateral thalamic nucleus (VPL) (Fig. 4D). In the midbrain, Id3 was expressed in the interpeduncular nucleus, rostral subnucleus (IPR) (Fig. 4E). On the other hand, the expression level of Id4 mRNA was low, and long exposure was required to obtain signals. Although we encountered high background, some regions were identified as positive for Id4 expression. In the main olfactory bulb, Id4 mRNA was expressed in the anterior commissure, intrabulbar part (aci), and glomerular layer (Gl) (Fig. 5A). In the caudate putamen, some cells were labeled (Fig. 5B). In the SVZ–ependymal region, some cells were labeled (Fig. 5B). Id4 mRNA expression

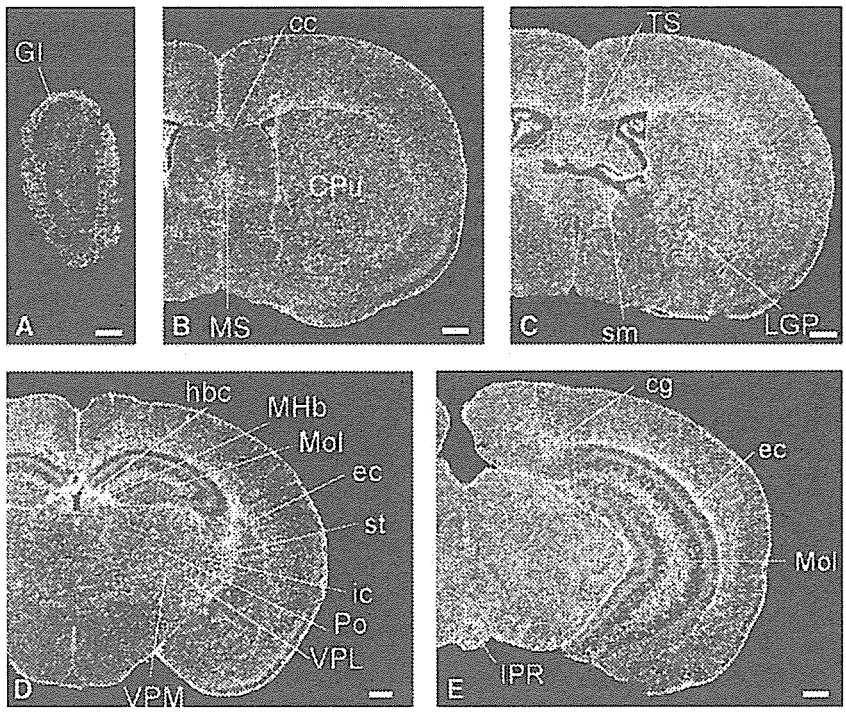

Fig. 4 – Id3 mRNA expression in the brain. Dark field photomicrographs showing Id3 mRNA expression in coronal sections. Strong expression was observed in the medial septal nucleus (B), stria medullaris of the thalamus (C), molecular layer of the dentate gyrus, external capsule, internal capsule (D), and cingulum (E). Scale bar, 500 m. Abbreviations are listed in Table 1.

was observed in the lateral amygdaloid nucleus dorsolateral part (LaDL), ventromedial part (LaVM), and medial amygdaloid nucleus posterodorsal part (MePD) (Fig. 5C). In the brainstem, Id4 mRNA was expressed in the interpeduncular nucleus, lateral and rostral subnuclei (IPL, IPR), and dorsal raphe nucleus, dorsal and ventral parts (DRD, DRV) (Fig. 5E). These

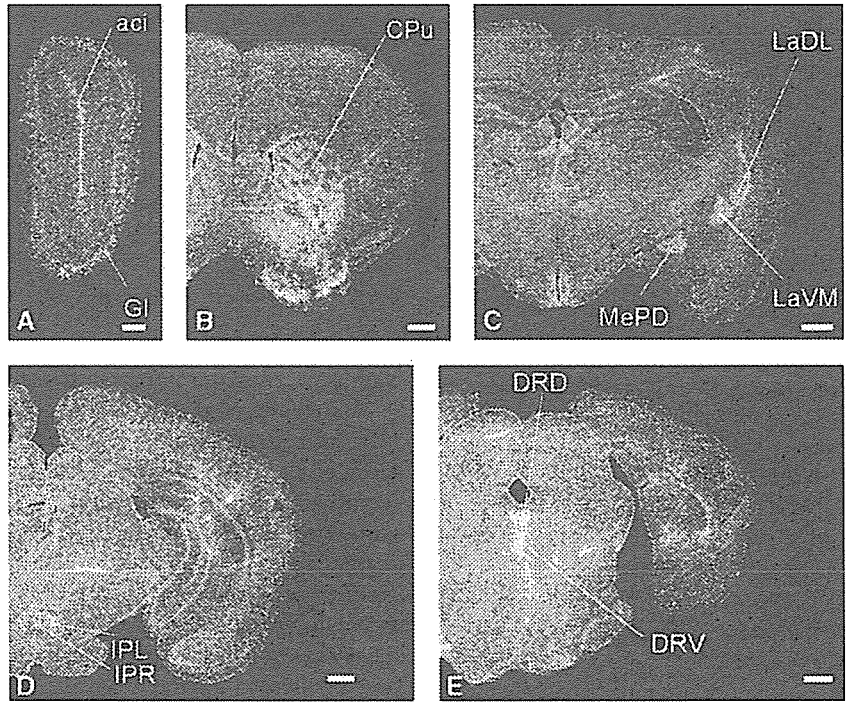

Fig. 5 – Expression of Id4 mRNA in the brain. Dark field photomicrographs showing Id4 mRNA expression in coronal sections. Expression was observed in the caudate putamen (B), lateral amygdaloid nucleus, dorsolateral and ventromedial part, medial amygdaloid nucleus, posterodorsal part (C), interpeduncular nucleus, lateral and rostral subnucleus (D), and dorsal raphe nucleus, dorsal and ventral parts (E). Scale bar, 500 m. Abbreviations are listed in Table 1.

Table 2 – Summary of Id2 and Id3 expression in the adult mouse brain

	Id2	Id3
Forebrain		
Main olfactory bulb		
Mitral cell layer	++	+
Glomerular layer	++	++
Granule cell layer	+	+
Anterior olfactory nucleus	+	+
Septum		
Lateral septal nucleus	+	+
Medial septal nucleus	–	++
Triangular septal nucleus	–	++
Corpus callosum	+[a]	++
Stria terminalis	–	++
External capsule	–	++
Internal capsule	–	++
Habenular commissure	–	++
Medial habenular nucleus	–	++
Cingulum	–	++
Cerebral cortex		
Neo cortex		
Layer 1	+[a]	+
Layer 2	++	+
Layer 3	++	+
Layer 4	–	+
Layer 5	+++	++
Layer 6	++	++
Amygdaloid complex		
Basolateral, anterior part	+++	+
Lateral		
Dorsolateral part	+++	+
Ventromedial part	+++	+
Ventrolateral part	+++	+
Medial		
Posterodorsal part	+++	+
Posteroventral part	+++	+
Anterior cortical	+++	+
Posteromedial cortical	+++	+
Intercalated nuclei	+++	+
Other subnuclei	++	+
Anterior amygdaloid area	++	+
Hippocampus		
Subgranular zone	++[a]	+
Subiculum	+++	+
Molecular layer	+[a]	+++
Nucleus of the lateral olfactory tract	++	+
Dorsal endopiriform nucleus	+++	+
Bed nucleus of stria terminalis	++	+
Intraamygdaloid division of the bed nucleus of the stria terminalis	++	+
Globus pallidus	++	++
Caudate putamen	+[a]	++[a]
Subventricular zone–ependymal region	++	++
Anterior part of the subventricular zone	+++	+
Ventral pallidum	++	+
Thalamus		
Ventral anterior nucleus	++	+
Ventral posteromedial nucleus	++	++[a]
Ventral posterolateral nucleus	–	++[a]
Posterior thalamic nuclear group	–	++[a]
Geniculate nucleus	++	+
Other subnuclei	+	+
Subthalamic nucleus	++	+
Hypothalamus		
Paraventricular hypothalamic nucleus anterior parvicellular part	++	+
Dorsomedial hypothalamic nucleus	++	+
Other nuclei	+	+
Suprachiasmatic nuclei	++	+
Midbrain		
Substantia nigra		
Pars compacta	–	+
Pars reticulata	++	+
Pars lateralis	–	+
Ventral tegmental area	–	+
Interpeduncular nucleus	++	++
Medial terminal nucleus of the accessory optic tract	+++	+
Red nucleus	++	+
Superior colliculus	++	+
Oculomotor nucleus	+	+
Trochlear nucleus	+	+
Pons		
Pontine nucleus	+++	+
Median raphe nucleus	+	+
Dorsal raphe nucleus	+	+
Periaqueductal gray	+	+
Pontine reticular nucleus, oral part	+	+
Lateral lemniscus	+++	+
Rostral periolivary region	+++	+
Nucleus of the trapezoid body	+++	+
Lateral superior olive	++	+
Periolivary region	++	+
Motor trigeminal nucleus	+	+
Principal sensory trigeminal nucleus	+	+
Lateral vestibular nucleus	++	+
Cochlear nuclei	+++	+
Medulla		
Lateral paragigantocellular nucleus	+	+
Rostroventrolateral reticular nucleus	+	+
Spinal trigeminal nucleus	+	+
Dorsal motor nucleus of the vagus	++	+
Hypoglossal nucleus	+	+
Cerebellum		
Purkinje cells	+++	+
Granule cell layer	–	+
Molecular layer	–	+
Cerebellar nuclei	++	+

Level of expression: +++ high; ++ moderate; + low; – not detected.
[a] Positive cells were scattered.

results revealed that the members of the Id gene family exhibit distinct expression patterns in the adult mouse brain.

The results of the present study are tabulated (Table 2). Since the expression levels of Id1 and Id4 were low, we excluded their results from the table. The present work thus confirmed the previous observations regarding the Id2 gene expression and further demonstrated that Id2 mRNA is distributed more widely throughout the brain. Our study provides evidence that supports the involvement of Id2 in neural functions of the adult brain. In addition, the results for expression of other Id genes imply that the Id gene products play distinct but overlapping roles in the adult mouse brain. Regarding the cell types that express Id2, morphological examination of the specimens counterstained by Nissl staining suggests that most of them are neurons. However, we cannot exclude the possibility that non-neuronal cells also express Id2, depending on the brain regions, because the

present study does not include double labeling with markers for neurons.

In the limbic system, Id2 mRNA was observed in various regions including the piriform, cingulate and retrosplenial cortices, septal nucleus, hippocampus, the bed nucleus of the stria terminalis, and many amygdaloid subnuclei. In the amygdala, Id2 mRNA is expressed moderately in LaDL and LaVM and highly in intercalated cells of the amygdala. The lateral nucleus is the main input station of the amygdala for visual and auditory sensory input (Collins and Pare, 1999; McDonald, 1998), and intercalated cell masses receive inputs from the basolateral complex and project to the central nucleus (Collins and Pare, 1999). Since the amygdala is associated with emotion and behavioral responses, Id2 may play a role in regulating these neural functions.

In the developing mouse brain, Id2 mRNA expression has a boundary in the neocortical layer 5, and the boundary demarcates the transition from the sensory to motor region, suggesting that Id2 is associated with cortical regionalization (Rubenstein et al., 1999). However, in the adult brain, the boundary is not clear in our analysis (data not shown). Id2 may have some function in addition to cortical regionalization. Id2 mRNA was expressed in the cranial nerve nuclei, not only in the motor nuclei, but also the sensory nuclei. As reported previously (Andres-Barquin et al., 2000; Jen et al., 1997; Neuman et al., 1991; Rubenstein et al., 1999; Tzeng and de Vellis, 1998), Id2 mRNA was observed in neurons in the cerebral cortex and caudate putamen. In addition, most cells in the globus pallidus and pars reticulata of the substantia nigra were labeled for Id2 mRNA. These observations suggest the involvement of Id2 in motor functions.

The circadian rhythm in mammals has been thought to be under the control of the pacemaker located in the SCN of the hypothalamus (Inouye and Shibata, 1994). As reported previously (Ueda et al., 2002), Id2 mRNA was detected in SCN in our study. In addition, we found that it was also expressed in the regions of the paraventricular nucleus (PVN) and stria terminalis (BNST). Vasopressin containing pathways from the SCN serve to affect neuroendocrine and autonomic neurons in the PVN (Buijs et al., 1998). GABA and glutamate are important mediators of fast monosynaptic transmission from the SCN to defined neurons in the PVN and are candidates for conveying circadian rhythmicity to PVN regulation of neuroendocrine and autonomic processes (Hermes et al., 1996). The circadian rhythm of electrical activity in the bed nucleus of the BNST is in phase with the SCN electrical activity rhythm (Yamazaki et al., 1998). Thus, Id2 may be involved in the regulation of circadian rhythm. In accordance with this notion, Id2 expression in the SCN is high during circadian night (Ueda et al., 2002).

It is known that two regions contain neural stem cells in the adult rodent brain: the subgranular zone (SGZ) of the hippocampal dentate gyrus and the subventricular zone (SVZ) (Altman and Bayer, 1990; Doetsch et al., 1999; Eriksson et al., 1998; Goldman, 1998; Johansson et al., 1999). The SGZ is the source of granule cells in the hippocampus produced during the juvenile and adult periods (Altman and Bayer, 1990), and the anterior part of the subventricular zone (SVZa) is a source of neuronal progenitor cells for the olfactory bulb (Luskin, 1993). In this study, we found that Id2 mRNA was expressed in the SVZa. Id2 may be related to the production of neurons in the olfactory bulb. This notion is consistent with the physiological activity of Id proteins because Id proteins are thought to function to expand and maintain the immature cells.

Acknowledgments

We are grateful to M. Sato for sharing equipment and D. Nathans and F. Sablitzky for materials. This work was supported by Grants-in-Aid and by the 21st Century COE program "Biomedical Imaging Technology Integration Program" from the Japan Society for the Promotion of Science.

REFERENCES

Altman, J., Bayer, S.A., 1990. Migration and distribution of two populations of hippocampal granule cell precursors during the perinatal and postnatal periods. J. Comp. Neurol. 301, 365–381.

Andres-Barquin, P.J., Hernandez, M.C., Israel, M.A., 2000. Id genes in nervous system development. Histol. Histopathol. 15, 603–618.

Benezra, R., Davis, R.L., Lockshon, D., Turner, D.J., Weintraub, H., 1990. The protein Id: a negative regulator of helix–loop–helix DNA binding proteins. Cell 61, 49–59.

Buijs, R.M., Hermes, M.H., Kalsbeek, A., 1998. The suprachiasmatic nucleus–paraventricular nucleus interactions: a bridge to the neuroendocrine and autonomic nervous system. Prog. Brain Res. 119, 365–382.

Christy, B.A., Sanders, L.K., Lau, L.F., Copeland, N.G., Jenkins, N.A., Nathans, D., 1991. An Id-related helix–loop–helix protein encoded by a growth factor-inducible gene. Proc. Natl. Acad. Sci. U. S. A. 88, 1815–1819.

Collins, D.R., Pare, D., 1999. Reciprocal changes in the firing probability of lateral and central medial amygdala neurons. J. Neurosci. 19, 836–844.

Doetsch, F., Caille, I., Lim, D.A., Garcia-Verdugo, J.M., Alvarez-Buylla, A., 1999. Subventricular zone astrocytes are neural stem cells in the adult mammalian brain. Cell 97, 703–716.

Elliott, R.C., Khademi, S., Pleasure, S.J., Parent, J.M., Lowenstein, D. H., 2001. Differential regulation of basic helix–loop–helix mRNAs in the dentate gyrus following status epilepticus. Neuroscience 106, 79–88.

Eriksson, P.S., Perfilieva, E., Bjork-Eriksson, T., Alborn, A.M., Nordborg, C., Peterson, D.A., Gage, F.H., 1998. Neurogenesis in the adult human hippocampus. Nat. Med. 4, 1313–1317.

Goldman, S.A., 1998. Adult neurogenesis: from canaries to the clinic. J. Neurobiol. 36, 267–286.

Hermes, M.L., Coderre, E.M., Buijs, R.M., Renaud, L.P., 1996. GABA and glutamate mediate rapid neurotransmission from suprachiasmatic nucleus to hypothalamic paraventricular nucleus in rat. J. Physiol. 496, 749–757.

Inouye, S.T., Shibata, S., 1994. Neurochemical organization of circadian rhythm in the suprachiasmatic nucleus. Neurosci. Res. 20, 109–130.

Ishii, K., Oda, Y., Ichikawa, T., Deguchi, T., 1990. Complementary DNAs for choline acetyltransferase from spinal cords of rat and mouse: nucleotide sequences, expression in mammalian cells, and in situ hybridization. Brain Res. Mol. Brain Res. 7, 151–159.

Jen, Y., Manova, K., Benezra, R., 1996. Expression patterns of Id1, Id2, and Id3 are highly related but distinct from that of Id4 during mouse embryogenesis. Dev. Dyn. 207, 235–252.

Jen, Y., Manova, K., Benezra, R., 1997. Each member of the Id Gene family exhibits a unique expression pattern in mouse gastrulation and neurogenesis. Dev. Dyn. 208, 92–106.

Johansson, C.B., Momma, S., Clarke, D.L., Risling, M., Lendahl, U., Frisen, J., 1999. Identification of a neural stem cell in the adult mammalian central nervous system. Cell 96, 25–34.

Kageyama, R., Nakanishi, S., 1997. Helix–loop–helix factors in growth and differentiation of the vertebrate nervous system. Curr. Opin. Genet. Dev. 7, 659–665.

Luskin, M.B., 1993. Restricted proliferation and migration of postnatally generated neurons derived from the forebrain subventricular zone. Neuron 11, 173–189.

Massari, M.E., Murre, C., 2000. Helix–loop–helix proteins: regulators of transcription in eucaryotic organisms. Mol. Cell. Biol. 20, 429–440.

McDonald, A.J., 1998. Cortical pathways to the mammalian amygdala. Prog. Neurobiol. 55, 257–332.

Mori, S., Nishikawa, S.I., Yokota, Y., 2000. Lactation defect in mice lacking the helix–loop–helix inhibitor Id2. EMBO J. 19, 5772–5781.

Neuman, T., Keen, A., Zuber, M.X., Kristjansson, G.I., Gruss, P., Nornes, H.O., 1991. Neuronal expression of regulatory helix–loop–helix factor Id2 gene in mouse. Dev. Biol. 160, 186–195.

Paxinos, G., Franklin, K., 2001. The Mouse Brain in Stereotaxic Coordinates, 2nd ed. Academic Press, San Diego, CA.

Riechmann, V., van Cruchten, I., Sablitzky, F., 1994. The expression pattern of Id4, a novel dominant negative helix–loop–helix protein, is distinct from Id1, Id2 and Id3. Nucleic Acids Res. 22, 749–755.

Rubenstein, J.L.R., Anderson, S., Shi, L., Miyashita-Lin, E., Bulfone, A., Hevner, R., 1999. Genetic control of cortical regionalization and connectivity. Cereb. Cortex 9, 524–532.

Ruzinova, M.B., Benezra, R., 2003. Id proteins in development, cell cycle and cancer. Trends Cell Biol. 12, 410–418.

Tzeng, S.F., de Vellis, J., 1998. Id1, Id2, and Id3 gene expression in neural cells during development. Glia 24, 372–381.

Ueda, H.R., Chen, W., Adachi, A., Wakamatsu, H., Hayashi, S., Takasugi, T., Nagano, M., Nakahama, K., Suzuki, Y., Sugano, S., Iino, M., Shigeyoshi, Y., Hashimoto, S., 2002. A transcription factor response element for gene expression during circadian night. Nature 418, 534–539.

Yamazaki, S., Kerbeshian, M.C., Hocker, C.G., Block, G.D., Menaker, M., 1998. Rhythmic properties of the hamster suprachiasmatic nucleus in vivo. J. Neurosci. 18, 10709–10723.

Yokota, Y., Mori, S., 2002. Role of Id family proteins in growth control. J. Cell. Physiol. 190, 21–28.

ELSEVIER

Journal of the Neurological Sciences 247 (2006) 109–111

Journal of the Neurological Sciences

www.elsevier.com/locate/jns

Short communication

Epileptic polyopia with right temporal lobe epilepsy as studied by FDG-PET and MRI: A case report

Takahiro Mitsueda-Ono [a], Akio Ikeda [a,*], Eri Noguchi [a], Shigetoshi Takaya [b], Hidenao Fukuyama [b], Shun Shimohama [a], Ryosuke Takahashi [a]

[a] *Department of Neurology, Kyoto University Hospital, 54 Shogoin-Kawaharacho, Sakyo-ku, Kyoto 606-8507, Japan*
[b] *Human Brain Research Center, Kyoto University School of Medicine, Japan*

Received 30 December 2005; received in revised form 14 April 2006; accepted 18 April 2006
Available online 21 June 2006

Abstract

Polyopia is one of rare, visual hallucinations. A 61-year-old man suffered from daily episodes of polyopia and generalized convulsions, and he was diagnosed as right temporal lobe epilepsy. MRI revealed right amygdalar swelling. FDG-PET showed hypometabolism in the right anterior temporal and the mesial occipital areas. Polyopia is thought to be caused by dysfunction of updating process of visual information in the visual association cortices. It was most likely that, in this patient, both mesial temporal and ipsilateral occipital areas were responsible for manifesting epileptic polyopia, as ictal onset zone and symptomatogenic zone, respectively.

Keywords: Polyopia; Partial epilepsy; Amygdala; FDG-PET

1. Introduction

Polyopia is one of complex visual hallucinations, manifesting appearance of plural images as erroneous visual perceptions even after the object has left out of visual field. On the other hand, palinopsia is also a kind of visual hallucinations, appearing plenty of the same images while watching one object [1]. Since this report, it was frequently reported referring to several neurological disorders, but it seems to involve temporo-occipital area commonly.

On the other hand, human "amygdalar epilepsy" is not established yet [2]. Amongst a series of 174 cases with intractable temporal lobe epilepsy (TLE) confirmed by video EEG monitoring, amygdalar enlargement was observed in seven patients (4%) [3].

Abbreviations: EEG, electroencephalography; MRI, magnetic resonance image; FDG, fluorodeoxyglicose; PET, positron emission computed tomography; TLE, temporal lobe epilepsy; AVM, artery venous malformation; FLAIR, fluid-attenuated inversion recovery.

Corresponding author. Tel.: +81 75 751 3772; fax: +81 75 751 9416.
E-mail address: akio@kuhp.kyoto-u.ac.jp (A. Ikeda).

0022-510X/$ - see front matter © 2006 Elsevier B.V. All rights reserved.
doi:10.1016/j.jns.2006.04.010

This is the first report that mentioned amygdalar enlargement and interictal PET study in epilepsy patients having polyopia. It may suggest that amygdala is also involved in manifesting polyopia as the ictal onset zone, but not necessarily as the symptomatogenic zone.

2. Case report

A 61-year-old right-handed man, without history of febrile convulsions, any developmental problems or head injury, was admitted because he had very frequent episodes of seeing "multiple, identical images previously seen" (called as polyopia as explained below) that were overlapped on his real vision mainly on the left side. He had several episodes of generalized convulsions with tongue bite since the age of 47 years, and he was free from generalized convulsions in the last 14 years, but the current type of visual symptoms started since age 60 years. Frequency of the current attacks has increased from once per 2 or 3 days to several times per day.

The polyopia episodes were elaborated as follows. He saw multiple, same persons who had been seen just before;

he had an episode while playing an aerobic dance and saw multiple same persons in front of him in a row who were actually playing side to him. On the other occasions, he saw some people around him whom he could not identify, and the experienced scene was accompanied. He felt as if he was moving along these people in the scene (Fig. 1), followed by ascending sensation of numbness on his trunk bilaterally. Each episode lasted about 10 s, and initially he was aware and he thought that he did not lose his consciousness. One of the authors witnessed the episode when he showed incoherent vocalization, oral and hand automatisms, no responsiveness and test words given during the episode were not remembered, being consistent with simple partial seizures followed by complex partial seizures. Once the visual symptoms started, he felt angry against and wanted to quit or overcome the episodes; otherwise, other emotional symptoms were not accompanied.

He has no family history of neurological diseases. General and neurological examinations revealed no abnormality in the interictal period. Interictal EEG showed intermittent irregular slow (2.5 to 3 Hz) activity in the right fronto-temporal area, and several sharp transients in the right midtemporal area once per several minutes. Ictal EEG was not recorded.

The right amygdala increased in size on MRI (Fig. 2a and b), and there were no gadolinium-enhanced lesions. The intensity in FLAIR images was not increased. Neither hippocampal atrophy nor sclerosis was detected on both sides. In FDG-PET study, there was regional glucose hypometabolism in the right temporal and in the caudal part along the calcarine fissure in the right medial occipital area (Fig. 3). As compared with healthy subjects by using SPM, regional glucose hypometabolism was significant in the right temporo-occipital area.

All neuropsychological examinations resulted in normal limits as follows: Wechsler Memory Scale: verbal 96, visual 117, general 103, attention 106, delay 96; Western Aphasia Battery: AQ 100, CQ 99.4; Raven's colored progressive matrices test: 32/37; Boston Naming Test: 48/60; Wechsler Adult Intelligence Scale-Revised: verbal IQ 131, performance IQ 136, total IQ 136.

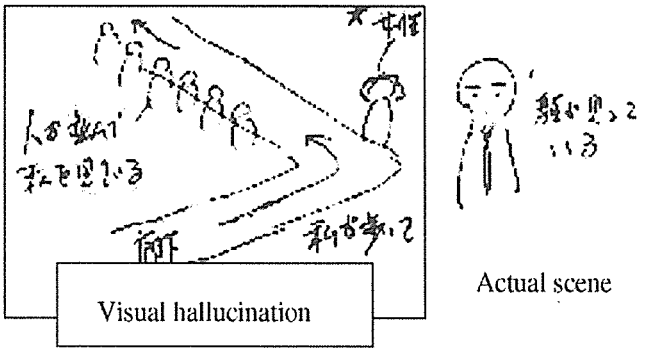

Fig. 1. One example of the polyopia drawn by the patient. While facing the doctor to whom he was talking, suddenly he felt as if he was walking along the corridor. Besides, he saw a row of the same unidentified persons and an unidentified woman who he just met before along the corridor. This visual hallucination appeared in the left visual field.

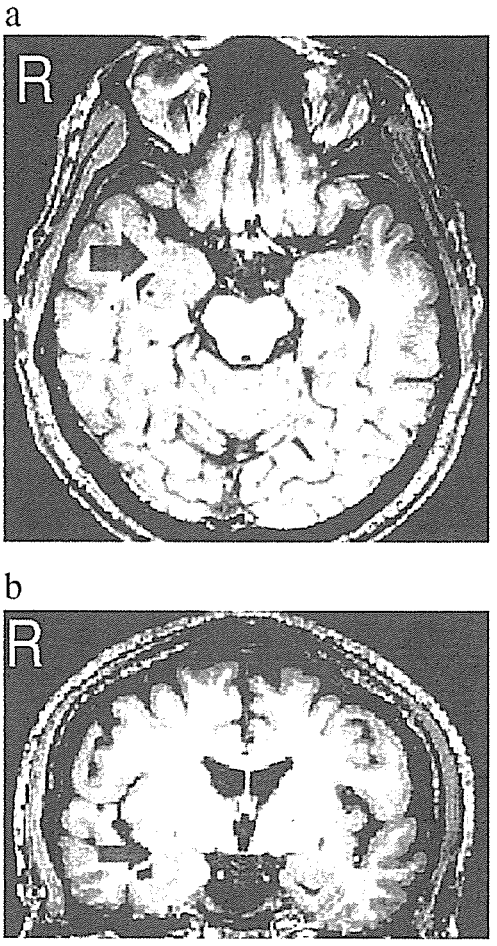

Fig. 2. T1-weighed MRI images. Right amygdalar enlargement was found in the axial (a) and the coronal (b) images. Arrow shows the enlarged amygdala.

We diagnosed him as right TLE based on ictal semiology, EEG, MRI and FDG-PET, and thus carbamazepine was started. It was gradually increased up to 300 mg/day, and his ictal symptoms have completely stopped.

3. Discussion

There were several reports that mentioned polyopia as seen in the present patient until now; however, it was rarely reported. According to those reports, it was observed in patients with cerebral infarction [1], head trauma [4], AVM [5], multiple sclerosis [6], non-ketoacidotic hyperglycemia [7], Creutzfeldt-Jakob disease [8] and migraine [9]. In case of partial epilepsy, occipitotemporal region or hippocampus was responsible [10].

From stimulation study, simple visual hallucination (e.g., light or scotoma) occurred by the stimulation of area 18 or 19 [11]. Lateral temporal lobe correlates with playback of sensory input. Stimulation of this region reminded patients of previously experienced scene [11].

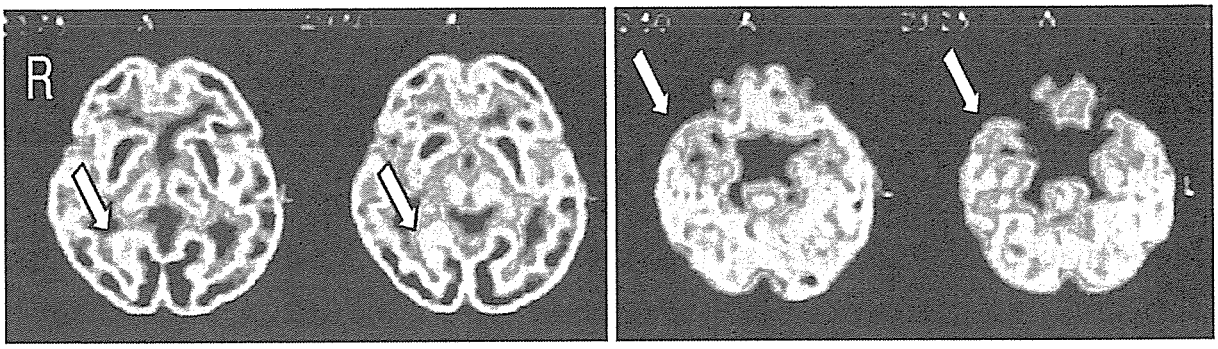

Fig. 3. PET study revealed hypometabolism in the right temporal lobe and right mesial occipital area (as shown by arrows).

In order to constitute polyopia, dysfunction of updating ongoing spatial perception in response to the circumstances would be necessary. It could occur by the impairment of not primary visual cortex but lateral temporal lobe, which correlates to record and accumulate visual perception. The responsible area for polyopia has remained unsolved; however, the abnormal input to the visual association cortex located in the temporo-occipito-parietal area could be one of the causes [12].

In the present patient, both right anterior temporal and mesial occipital areas were involved according to FDG-PET study. Hypometabolic brain areas as revealed by FDG-PET indicate not only epileptogenic but also symptomatogenic brain regions [13]. Hence, these two regions are involved as either symptomatogenic or epileptogenic zone. Right anterior temporal area (frequent interictal spikes in interictal EEG), especially the swollen right amygdala, most likely plays an important role as epileptogenic zone.

Amygdalar enlargement is a distinct entity from mesial temporal sclerosis. When we consider medial temporal lobe epilepsy, it is necessary to pay attention to amygdalar abnormality. Abnormal EEG discharges with amygdalar enlargement that acts as epileptogenic zone can lead to ipsilateral occipital area as symptomatogenic zone. This finding also suggests the connection between amygdala and occipital lobe. Additionally, it is also noteworthy that polyopia can manifest even in patients with TLE since an epileptogenic zone could be distant from the symptomatogenic zone of polyopia.

Acknowledgement

This study was supported by the Research Grant for the Treatment of Intractable Epilepsy (16-1) from the Japan Ministry of Health, Labor and Welfare, and a Scientific Research Grant (C2) 18590935 from the Japan Society for Promotion of Sciences.

References

[1] Critchley M. Types of visual preservation: "palinopsia" and "illusory visual spread". Brain 1951;74:267–99.
[2] Wieser HG. Mesial temporal lobe epilepsy versus amygdalar epilepsy: late seizure recurrence after initially successful amygdalotomy and regained seizure control following hippocampectomy. Epileptic Disord 2000;2:141–51.
[3] Bower SPC, Vorgin SJ, Morris K, Cox I, Murphy M, Kilpatrick CJ, et al. Amygdala volumetry in "imaging-negative" temporal lobe epilepsy. J Neurol Neurosurg Psychiatry 2003;74:1245–9.
[4] Kinsbourne M, Warrington EK. A study of visual preservation. J Neurol Neurosurg Psychiatry 1963;26:468–75.
[5] Jacobs L. Visual allesthesia. Neurology 1980;30:1059–63.
[6] Jacome DE. Palinopsia and bitemporal visual extinction on fixation. Ann Ophthalmol 1985;17:251–2.
[7] Johnson SF, Loge RV. Palinopsia due to nonketotic hyperglycemia. West J Med 1988;148:331–2.
[8] Purvin V, Bonnin J, Goodman J. Palinopsia as a presenting manifestation of Creutzfeldt-Jacob disease. J Clin Neuroophthalmol 1989;9:242–8.
[9] Klee A, Willanger R. Disturbances of visual perception in migraine: review of the literature and a report of eight cases. Acta Neurol Scand 1966;42:400–14.
[10] Christian GB, Felix OB, Horst U, Johannes S, Martin K, Christian EE. Localizing value of epileptic visual auras. Brain 2000;123:244–53.
[11] Penfield W, Perot P. The brain's record of auditory and visual experience. Brain 1963;86:596–696.
[12] Okada K, Akamatsu N, Hashimoto T, Uozumi T, Tsuji S. A case of right mesial temporal lobe epilepsy accompanied with ictal polyopsia. Clin Neurol 2004;44:39–42 [Only abstract written in English].
[13] Schlaug G, Antke C, Holthausen H, Arnold S, Ebner A, Tuxhorn I, et al. Ictal motor signs and interictal regional cerebral hypometabolism. Neurology 1997;49:341–50.

ELSEVIER

Clinical Neurophysiology 117 (2006) 1481–1486

www.elsevier.com/locate/clinph

Generators and temporal succession of giant somatosensory evoked potentials in cortical reflex myoclonus: Epicortical recording from sensorimotor cortex

Takefumi Hitomi [a], Akio Ikeda [a,*], Riki Matsumoto [a], Masako Kinoshita [a], Junya Taki [b], Keiko Usui [c], Nobuhiro Mikuni [b], Takashi Nagamine [c], Nobuo Hashimoto [b], Hiroshi Shibasaki [d], Ryosuke Takahashi [a]

[a] *Department of Neurology, Kyoto University Graduate School of Medicine, Kyoto, Japan*
[b] *Department of Neurosurgery, Kyoto University Graduate School of Medicine, Kyoto, Japan*
[c] *Department of Brain Pathophysiology, Human Brain Research Center, Kyoto University Graduate School of Medicine, Kyoto, Japan*
[d] *Takeda General Hospital, Kyoto, Japan*

Accepted 29 March 2006

Abstract

Objective: To clarify the generator mechanism of giant somatosensory evoked potentials (giant SEPs) and the hyperexcitability of primary somatosensory and motor cortices (SI and MI).

Methods: In a patient with intractable focal seizures manifesting cortical reflex myoclonus of the left foot, giant SEPs to left tibial nerve stimulation were epicortically recorded as a part of presurgical evaluation with subdural electrodes.

Results: In the single pulse SEPs, enlarged P1–N1 components were observed at the foot area of the SI and MI (86.5–258.8 μV, respectively), and the peak latencies were always shorter at SI than at MI by 6 ms. Similar findings were obtained for peroneal and sural nerve stimulation. In the paired pulse SEPs, the second response was less suppressed, as compared to other interstimulus intervals (ISIs), with ISIs of 40 and 200 ms both at SI and MI.

Conclusions: In this particular patient, cortical hyperexcitability to somatosensory stimuli seems to originate from SI but subsequently both SI and MI are responsible for the generation of giant SEPs and cortical reflex myoclonus.

Significance: Somatosensory and primary motor cortices both generated enhanced early cortical components of SEPs, most likely by enhancing the latter by the former.

Keywords: Giant somatosensory evoked potential (giant SEP); Cortical reflex myoclonus; Primary somatosensory cortex (SI); Primary motor cortex (MI)

1. Introduction

Extremely enlarged cortical components of somatosensory evoked potentials (giant SEPs) are observed in the majority of patients with cortical reflex myoclonus. The giant SEPs are considered to represent the degree of cortical hyperexcitability of the primary sensorimotor cortices (SMI) in response to somatosensory stimuli (Shibasaki et al., 1985), and are considered to result from pathological enhancement of certain early components of normal SEPs (Ikeda et al., 1995; Kakigi and Shibasaki, 1987a; Shibasaki

Abbreviations: SEP, somatosensory evoked potential; SMI, primary sensorimotor cortices; SI, primary somatosensory cortex; MI, primary motor cortex; ISI, interstimulus interval; SEP-R, SEP recovery function; ECoG, electrocorticogram; MEG, magnetoencephalography; SEF, somatosensory evoked magnetic field.

* Corresponding author. Address: Department of Neurology, Kyoto University Hospital, 54 Shogoin-Kawaharacho, Sakyo-ku, Kyoto 606-8507, Japan. Tel.: +81 75 751 3772; fax: +81 75 751 9416.

E-mail address: akio@kuhp.kyoto-u.ac.jp (A. Ikeda).

1388-2457/$30.00
doi:10.1016/j.clinph.2006.03.029

et al., 1990). As for the generator mechanism of giant SEPs, previous study by means of simultaneous recording of SEPs and somatosensory evoked magnetic fields (SEFs) showed that abnormal hyperexcitability involves both primary somatosensory and motor cortices (SI and MI, respectively) (Mima et al., 1998). However, the generator sources of giant SEPs have not been fully understood.

In the present study, we investigated the giant SEPs recorded from chronically implanted subdural electrodes in order to clarify the generator mechanism and the hyperexcitability of SI and MI in a patient with intractable focal epilepsy manifesting cortical reflex myoclonus. Only the abstract for this objective appeared elsewhere (Hitomi et al., 2004), and other electrophysiological and clinical features of the patient are described elsewhere for an entirely different purpose (Matsumoto et al., 2005; Mikuni et al., 2005; Nakagawa et al., in press).

2. Patient and methods

A 31-year-old man had intractable focal seizures and cortical reflex myoclonus involving the left foot due to focal cortical dysplasia in the right parasagittal central region. The patient was on many kinds of anticonvulsants, such as carbamazepine (800 mg/day), phenytoin (300 mg/day), phenobarbital (80 mg/day), zonisamide (700 mg/day) and clobazam (10 mg/day). By video-EEG monitoring, the epileptogenic zone was defined at and very close to the foot area of the right SI and MI. Clinically he had both positive and associated negative myoclonus and showed an enhanced long-loop transcortical reflex (C-reflex) to electrical stimulation of the left foot. Before implantation of the subdural electrodes, SEFs in response to stimulation of bilateral tibial nerves were recorded (passband: 0.07–200 Hz, sampling rate: 901 Hz) in the magnetically shielded room with the 122 first-order planar SQUID gradiometers (Neuromag122, Neuromag, Helsinki, Finland).

2.1. Scalp SEPs

Scalp SEPs in response to stimulation of bilateral tibial and sural nerves were recorded before implantation of the subdural electrodes and 20 days after the resective surgery. The electrical stimulus was presented as a constant voltage square-wave pulse of 0.2 ms duration, and interstimulus interval (ISI) was set to 2.9 s. It was delivered to the tibial nerve at the ankle and to the sural nerve below the lateral malleolus. Stimulus intensity was adjusted to 120% of motor threshold so as to produce a clear twitch of the hallux for the tibial nerve and to 300% of sensory threshold for the sural nerve. The scalp electrodes were placed at Fz, Cz and Pz based on the 10–20 International System, and were also placed at CPz, CP3 and CP4 defined as the midway between each corresponding pair of electrodes. All electrodes were referred to the linked earlobes (A1 + A2). The bandpass filter of the amplifier was set to 1.6–3000 Hz, and sampling rate was set to 10,000 Hz. Three hundred responses for each session were averaged and at least two sets were recorded to confirm the reproducibility of the waveforms.

2.2. Epicortical SEPs

Single and paired pulse SEPs were recorded from subdural electrodes while the patient was undergoing invasive seizure monitoring and functional mapping. Informed consent was obtained based on the Clinical Research Protocol No. 79, approved by the Committee of Medical Ethics, Kyoto University Graduate School of Medicine. Single pulse SEPs were recorded by stimulation of the left tibial, peroneal and sural nerves. The condition of electrical stimulation for the left tibial and sural nerves were the same as those for the scalp SEP recording except for shorter ISI (1 s) in the epicortical recording. As for the left peroneal nerve, stimulus was delivered on the skin over the left fibular head and stimulus intensity was adjusted to 120% of motor threshold of the tibialis anterior muscle. All subdural electrodes were referred to the skin electrode on the left mastoid process. All other recording conditions were the same as those for scalp SEP recording.

Recovery functions of SEP response were studied by giving paired stimuli with various ISIs. Each pair of stimuli was delivered once every 3 s or longer. ISIs were set to 30, 40, 60, 80, 100, 120, 140, 160 and 200 ms. In order to maintain the same recording condition among different ISIs, stimuli with different ISIs were randomly delivered in the same recording session, and the single pulse stimuli were also intermixed among them. The SEP recovery function (SEP-R) of P1–N1 and N1–P2 components of the response to the second stimuli (SEP2) was calculated with respect to the response to the first stimuli (SEP1) for each ISI. Cortical excitability was judged to be non-suppressed when the ratio of SEP2/SEP1 was 100% or larger for both SI and MI. For statistical analysis, the Mann–Whitney U test was employed to compare the ratio of SEP2/SEP1 between non-suppressed ISIs data and suppressed one. The level of significance was set with P value of less than 5%.

3. Results

3.1. Scalp SEPs

Scalp SEPs following the left tibial nerve stimulation showed maximal cortical responses at CPz. As for the latencies, peaks of SEPs to the left foot stimulation were delayed (P1: 51.6 ms, N1: 63.8 ms and P2: 103.0 ms) as compared with the right foot stimulation (P1: 42.7 ms, N1: 55.8 ms and P2: 65.4 ms) (Table 1A, Fig. 1A and B). With regard to the amplitudes, P1–N1 and N1–P2 components for the left foot stimulation (P1–N1: 15.0 uV and N1–P2:

Table 1

Nerve	Electrode	Latency (ms)			Amplitude (μV)		
		P1	N1	P2	Baseline-P1	P1–N1	N1–P2
A scalp SEP							
Left tibial	CPz	51.6	63.8	103.0	6.0	15.0	17.1
Right tibial	CPz	42.7	55.8	65.4	0.1	3.6	2.7
Left sural	CPz	54.6	70.2	158.5	2.2	9.7	17.1
Right sural	CPz	50.1	61.4	135.0	0.1	3.0	8.6
B subdural SEP							
Left tibial	A19 (SI)	45.0	59.5	73.2	46.2	207.2	152.3
	B3 (MI)	49.6	64.8	82.4	2.4	86.5	86.6
Left peroneal	A19 (SI)	38.1	51.6	83.5	14.0	125.5	156.1
	B3 (MI)	43.8	59.9	88.2	47.3	258.8	276.8
Left sural	A19 (SI)	43.5	62.1	95.2	25.9	120.8	92.9
	B3 (MI)	49.1	68.7	97.2	32.0	104.5	102.1

17.1 μV) were about 4 times larger than those for the right foot stimulation (P1–N1: 3.6 μV and N1–P2: 2.7 μV) (Table 1A, Fig. 1A and B). P1–N1 for the left tibial nerve stimulation was compatible with 'giant' SEPs according to the previous study (P1–N1 amplitude being more than 11.4 μV (mean+3SD)) (Kakigi and Shibasaki, 1987b). As for the sural nerve stimulation, cortical components also showed delayed latencies and increased amplitudes to the left foot stimulation as compared with the right foot stimulation (Table 1A).

Twenty days after the resective surgery, scalp SEPs were recorded again. As for SEPs to the left tibial nerve stimulation, peak latencies (P1: 53.4 ms, N1: 70.2 ms and P2: 108.3 ms) were still delayed and amplitude of P1–N1 component (11.2 μV) was larger than that for the contralateral stimulation (2.4 μV). However, its amplitude

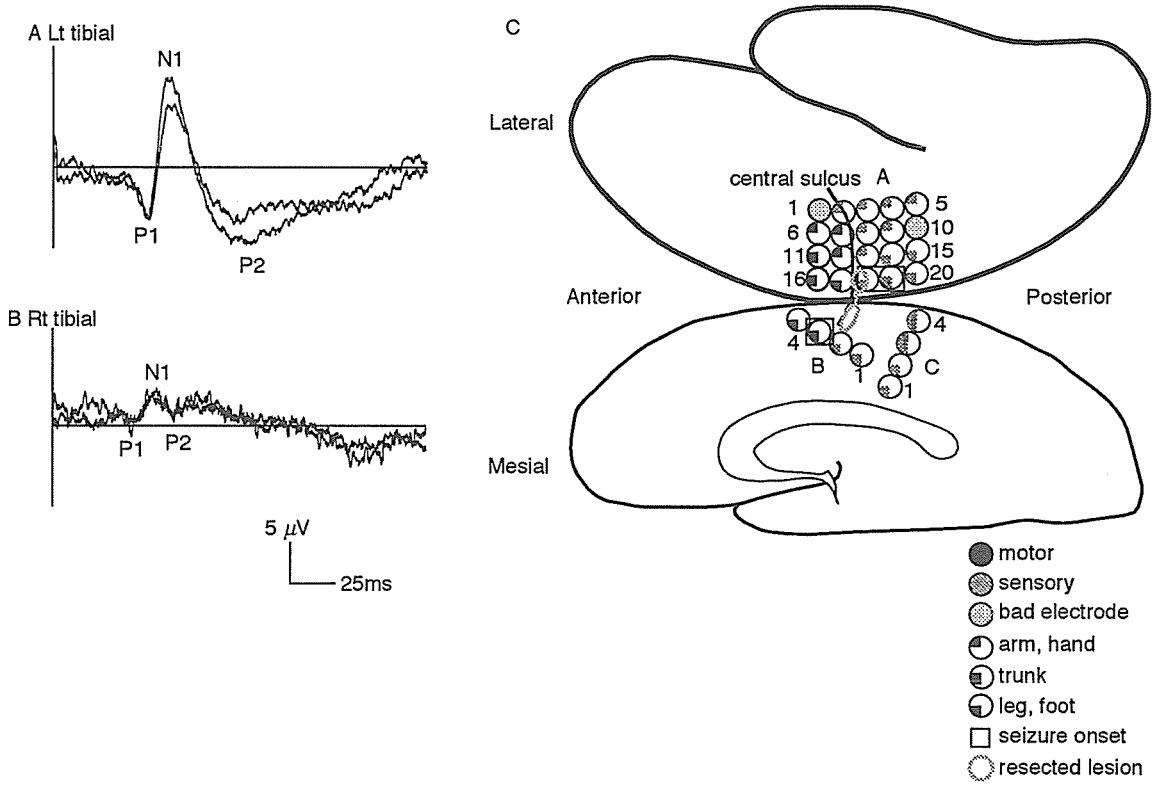

Fig. 1. Scalp recorded SEP waveforms at CPz to the left (A) and right (B) tibial nerve stimulation and the results of invasive functional mapping (C). In C, cortical functions beneath each subdural electrode are shown by symbols. B3, A18 and A19, as surrounded by bold squares, were defined as seizure onset area. Interictal spikes were frequently recorded at B2, B3, A18 and A19. A17, B3 and B4 corresponded to the foot or leg motor cortex, and A14, 15, 18-20, B1, 2 and C 1–4 corresponded to that of sensory cortex as determined by electrical stimulation. Gray bold circle and line indicated that the resected epileptogenic area of the cortical dysplasia was located in the posterior portion of the post-central gyrus reaching to the bottom of the right central sulcus.

became smaller in spite of the presence of craniotomy as compared with one before surgery.

As for the comparison between the scalp SEPs and SEFs to the left tibial nerve stimulation, peak latencies of P1 and N1 components at CPz were similar to those of SEFs (P1: 50.4 ms, N1: 62.4 ms).

3.2. Epicortical SEPs

Enhanced cortical components were recorded at A18 and A19 (SI) and at B3 (MI) (Fig. 1C). SEP waveforms among the 3 stimulated nerves (tibial, peroneal and sural) were similar in the latency of P1 and N1, and P1–N1 amplitude was equally enlarged (Table 1B). The peak latencies of the left peroneal nerve SEPs were shorter by 5–7 ms than those of tibial and sural nerve SEPs, since the former was stimulated at the fibular head whereas the latter two were stimulated at the ankle.

There was a consistent latency difference of each peak between SI and MI, although the waveforms of cortical components at SI (A19) and MI (B3) were similar (Fig. 2). Peak latencies of each component (P1, N1, P2) at SI (A19) were shorter than those at MI (B3) by about 6 ms on average (mean $\pm$SD: 5.8 $\pm$2.1; ranging from 2.0 to 9.2); left tibial (6.4 $\pm$2.8; 4.6–9.2), peroneal (4.7 $\pm$2.4; 2.0–5.6) and sural (6.2 $\pm$1.9; 4.7–8.3). Peak latencies at SI (B2) were also shorter than those at MI (B3) by about 6 ms (6.0 $\pm$2.3; 2.0–9.9) despite the proximity of the recording site (Fig. 2). The P1–N1 amplitudes at both SI (A19) and MI (B3) were equally enhanced for the left tibial, peroneal and sural nerve stimulation (Table 1B).

The comparison between scalp and epicortical SEPs to the left tibial nerve stimulation showed similar morphology of P1 and N1 components, but the late components including P2 were different (Fig. 2A). A similar tendency was observed for the left sural nerve stimulation (Fig. 2B). Peak latencies of P1 and N1 components at CPz were longer than those at SI (A19) by about 4–11 ms to the left tibial (P1: 6.6 ms, N1: 4.3 ms) and sural (P1: 8.1 ms, N1: 11.1 ms) nerve stimulation. By contrast, the time difference between MI (B3) and CPz was much less than that between SI and CPz; left tibial (P1: 2.0 ms, N1: 1.0 ms) and sural (P1: 5.5 ms, N1: 1.5 ms) nerve stimulation (Table 1, Fig. 2).

As for the SEP-R of P1–N1 and N1–P2 components, the SEP2 was less than 100% of the SEP1 at SI (A19) and MI (B3) with all the ISIs examined in the present study (Fig. 3), as judged by normal range (within mean $\pm$3SD of those obtained from normal subjects) in previous scalp-recorded, paired SEP study (Ugawa et al., 1991). In detail, the SEP2 was less than 60% of the SEP1 at SI (A19) and MI (B3) at ISI of 30–200 ms except for the ISIs of 40 ms (80.7% at SI and 92.0% at MI for P1–N1 component, 94.5% at SI and 82.4% at MI for N1–P2 component) and of 200 ms (77.2% at SI and 63.0% at MI, 94.5% at SI and 91.3% at MI) (Fig. 3). The degree of

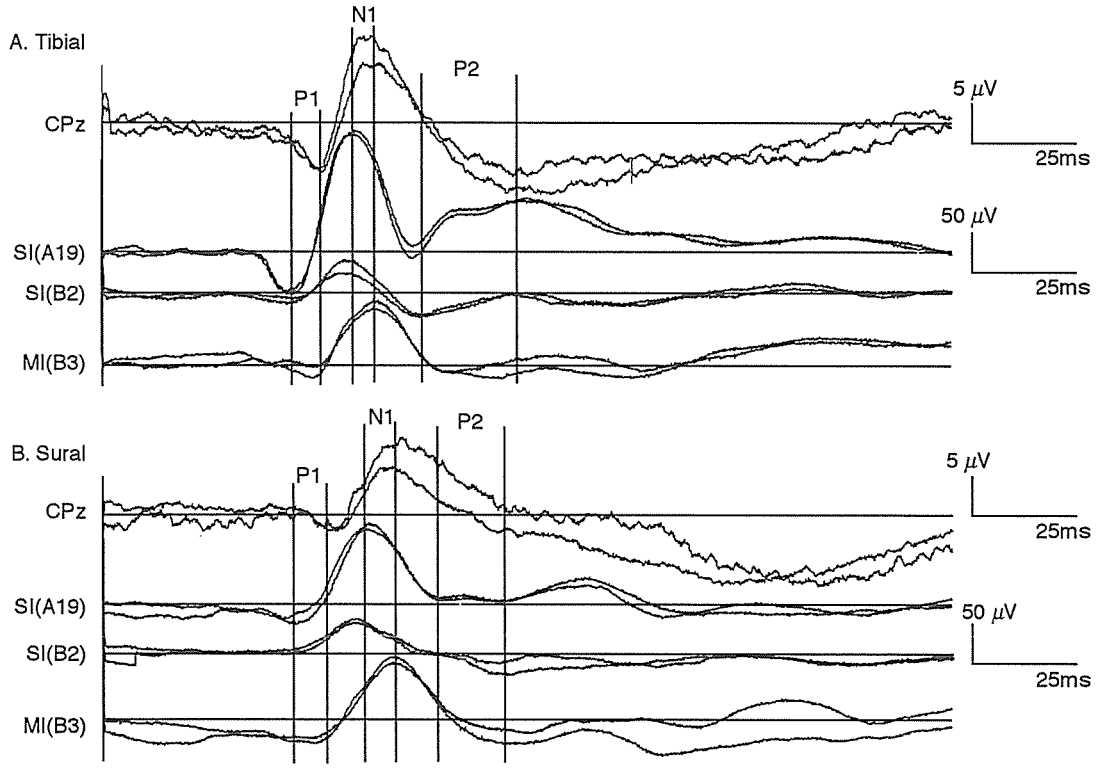

Fig. 2. Scalp (CPz) and subdurally (SI and MI) recorded SEPs to the left tibial (A) and sural (B) nerve stimulation. Vertical solid lines show peaks of each component (P1, N1, P2) at CPz and vertical dotted lines show those at SI (A19 and B2) to the left tibial and sural nerve stimulation. The peak latencies were consistently longer at MI as compared with SI, and the latencies at MI were similar to those at CPz.